Quarterly Reviews of Biophysics **33**, 4 (2000), pp. 371–424. Printed in the United Kingdom

NMR structures of biomolecules using field oriented media and residual dipolar couplings

J. H. Prestegard[1]*, H. M. Al-Hashimi[1,2] and J. R. Tolman[3]

[1] Complex Carbohydrate Research Center, University of Georgia, Athens, GA, USA
[2] Department of Chemistry, Yale University, New Haven, CT, USA
[3] Section de Chimie, Université de Lausanne, BCH, CH-1015 Lausanne, Switzerland

* Author to whom correspondence should be addressed.

https://doi.org/10.1017/S0033583500003656 Published online by Cambridge University Press

1. Introduction

1.1 Residual dipolar couplings as a route to structure and dynamics

Within its relatively short history, nuclear magnetic resonance (NMR) spectroscopy has managed to play an important role in the characterization of biomolecular structure. However, the methods on which most of this characterization has been based, Nuclear Overhauser Effect (NOE) measurements for short-range distance constraints and scalar couplings measurements for torsional constraints, have limitations (Wüthrich, 1986). For extended structures, such as DNA helices, for example, propagation of errors in the short distance constraints derived from NOEs leaves the relative orientation of remote parts of the structures poorly defined. Also, the low density of observable protons in contact regions of molecules held together by factors other than hydrophobic packing, leads to poorly defined structures. This is especially true in carbohydrate containing complexes where hydrogen bonds often mediate contacts, and in multi-domain proteins where the area involved in domain–domain contact can also be small. Moreover, most NMR based structural applications are concerned with the characterization of a single, rigid conformer for the final structure. This can leave out important mechanistic information that depends on dynamic aspects and, when motion is present, this can lead to incorrect structural representations. This review focuses on one approach to alleviating some of the existing limitations in NMR based structure determination: the use of constraints derived from the measurement of residual dipolar couplings (D).

https://doi.org/10.1017/S0033583500003656 Published online by Cambridge University Press

There are many anisotropic interactions in NMR that contain valuable structural information, but residual dipolar couplings have, in practice, been the measurement of choice. As will be discussed in Section 2, residual dipolar couplings originate from the anisotropic component of the dipolar interaction, a component dependent on the angle between an internuclear vector and the magnetic field, as $(3\cos^2\theta - 1)$. These interactions are not normally directly observable in high resolution NMR because anisotropic interactions effectively average to zero with molecular tumbling. However, they can be seen as splittings of resonances (or contributions to existing splittings) if small degrees of molecular order are induced. The angular dependence of these couplings can then provide valuable structural constraints on the relative orientation of even spatially remote parts of molecules under study.

Since numerous pairwise dipolar interactions between magnetic nuclei exist in a single molecule, one may wonder why the measurement of residual dipolar couplings in macromolecules rose to prominence only recently. One reason is the requirement for not only the introduction of molecular order but the introduction of a proper level of molecular order. For applications to macromolecular systems, this order must be small enough to avoid unmanageable complexity, must occur without compromising resolution, and must use a compatible solvent system. This required the advent of dilute aqueous liquid crystal media and the engineering of properties to improve stability and the control of interactions between medium and solute. We discuss some of the advances in medium development in Section 3.

Once a suitable level of order is induced, it is very straightforward to measure residual dipolar couplings both efficiently and accurately. In simpler systems, measurements can be made directly from splittings of resonances in the frequency domain, just as scalar coupling measurements have been made for decades. However, the need for precise measurement, and the need to simultaneously deal with large numbers of interactions in macromolecular systems, have also led to the development of more sophisticated procedures. Combined with the availability of stable isotope labeling techniques, residual dipolar couplings can now be obtained with little effort even in macromolecular systems. In Section 4, we consider some of the fundamental techniques that have been developed for the measurement of residual dipolar couplings in both isotopically labeled and non-labeled samples.

To make full use of the rapidly growing pool of residual dipolar coupling data, modifications to existing structural determination protocols are required. In Section 5 we consider two evolving methods; one based on simulated annealing in the presence of penalty functions, and another which seeks to determine the orientation of molecular fragments of known local geometry directly from residual dipolar coupling data. The relative advantages depend on the system under study, and the amount and type of information available at the onset of structure determination. Using these methods, it is already clear that the inclusion of orientational constraints during structural refinement leads to improvement in the quality of structures determined by NMR. Recent developments indicate that structure determination in the near absence of NOEs may soon be possible. In Section 6, we discuss some of these structural applications in more detail.

Thus far the primary focus of the biological community has been on structural applications, with only a few studies seeking to exploit the sensitivity of residual dipolar couplings to dynamics. However, as better means of alignment are devised and precision of measurement improves, the effects of dynamics will become an issue. On the one hand, this provides an exciting avenue of exploration, since typical residual dipolar coupling measurements are sensitive to all dynamic processes occurring on timescales shorter than

100 ms. On the other hand, direct structural analysis may be impeded by the presence of motional effects, and techniques to separate the structural and dynamic contributions to residual dipolar couplings will become important. We therefore have included a discussion of dynamics in the theoretical section that begins this review.

1.2 A brief history of oriented phase high resolution NMR

Before we begin, it is appropriate to point out that the basic ideas behind application of residual dipolar coupling measurements to the study of molecular structure and dynamics are not new. In 1963, Saupe and coworkers realized that by dissolving small molecules in nematic solvents they could reintroduce anisotropic interactions in high resolution NMR spectra (Saupe & Englert, 1963). In a classic example, they used an organic solvent called *p*-azoxyanisole and benzene as a solute. The ^{1}H spectrum of benzene no longer displayed a single peak, but rather, was a complex spectrum of 50 or more lines. Moreover, the resolution of the solute spectrum was retained, and any signals from the nematic solvent disappeared in the background.

The term 'nematic' (from the Greek word for thread), was used to describe the rod-like shape of the solvent molecules which possessed anisotropic magnetic susceptibilities, and which cooperatively formed a homogenous but anisotropic medium when under the influence of a moderate magnetic field. The term 'nematic' is now also used to distinguish media from others by the fact that a nematic solvent is disordered in all but a single direction. The complexity of the benzene spectrum dissolved in a nematic medium resulted from intramolecular dipole–dipole interactions that normally average to zero in an isotropic medium, and the high resolution spectrum was retained due to the reduction of intermolecular dipole–dipole interactions (compared to the solid state) by rapid translational diffusion. This compromise between high resolution NMR and solid state NMR lead to what is commonly referred to as liquid crystal NMR (Emsley & Lindon, 1975).

These earlier studies set the stage for structural interpretation of residual dipolar couplings. One major obstacle to structural applications was interpretation of the average angular dependence of residual dipolar couplings given by the quantity $\langle(3\cos^2\theta-1)/2\rangle$, where θ is the angle between the internuclear vector and the magnetic field, and the angle brackets denote averaging due to molecular reorientation. Extraction of structural information would appear to require complete knowledge of the distribution function governing molecular orientation. Saupe, Snyder, Buckingham and Pople recognized that, because this angular dependence is a second rank spherical harmonic, the relevant part of the probability distribution could be expressed as a linear combination of just the five elements of second rank spherical harmonics (Buckingham & Pople, 1963; Saupe, 1964; Snyder, 1965). Hence, measurement of five or more suitably independent residual dipolar couplings in a known rigid element would permit extraction of structural information. As we discuss in Sections 2 and 4, these five spherical harmonics are directly related to the five elements of what is commonly referred to as the alignment tensor, and is the basis for the order matrix approach to extracting structural information.

Despite these advances, application of liquid crystal techniques to the measurement of anisotropic interactions in macromolecules remained problematic. While spectra of small molecules could be analyzed, spectra of larger systems became intractable because of the

hundreds of resonances produced. A further scaling and filtering of resonances was required. Ironically, the first applications of residual dipolar couplings for structural analysis of macromolecules did not emerge from the use of liquid crystalline media, but from the direct alignment of solute molecules at high magnetic fields (Bastiaan & MacLean, 1990; Bastiaan *et al.* 1987). It was recognized that molecules with sufficiently large magnetic susceptibility anisotropies would adopt preferred orientations in magnetic fields. The size of induced magnetic moments in such molecules, and hence the energy of interaction with the magnetic field, would vary with orientation and produce non-isotropic distributions. The first observation of magnetic alignment was made in 1978 by Lohman and Maclean (Lohman & MacLean, 1978). They observed quadrupolar splittings in magnetically aligned d_6-benzene (quadrupolar splittings display the same $(3\cos^2\theta - 1)$ dependence as residual dipolar couplings, but are larger in magnitude).

The observation of residual dipolar couplings under direct field induced orientation awaited the advent of higher fields (in these weak, non-cooperative, orientation limits, contributions to splittings scale with the field squared). In 1981, Bothner-By and co-workers were first able to measure the smaller residual dipolar interaction in the paramagnetic system bis[tolyltris(pyrazlyl)borato]cobalt(II) ($Co(TTPB)_2$), where magnetic alignment is almost an order of magnitude larger than in diamagnetic systems (Bothner-By *et al.* 1981). They also then made the first move toward applications in biologically relevant systems with measurements of quadrupolar and residual dipolar measurements in porphyrin and nucleic acid systems, where anisotropy in susceptibility is diamagnetic in origin (Bothner-By, 1995; Lisicki *et al.* 1988).

The first application to a protein relied on a combination of direct field induced orientation and the availability of a ^{15}N labeled protein. The combination of the low level of alignment produced by direct field induced alignment, the low gyromagnetic ratio of ^{15}N (about one tenth that of a proton), and the ability to observe couplings through the ^{15}N resonances, all contributed to the necessary spectral simplification. The measured residual dipolar contributions to the scalar one bond ^{15}N–^{1}H couplings only reached 2·5 Hz, even at the 17 T fields of a 750 MHz spectrometer available at the time (Tolman *et al.* 1995). However, these measurements agreed sufficiently well with values predicted from X-ray derived geometries to demonstrate structural utility in macromolecules. As we will discuss in Sections 3, other examples of applications relying on large anisotropic susceptibilities in macromolecules have followed, and there has been a considerable effort to artificially amplify magnetic anisotropies in macromolecules so that the direct approach to alignment can be used.

In practice, not many macromolecules have large magnetic anisotropies, making the level of alignment small and limiting the number of residual dipolar coupling measurements that can be made with confidence. A very important step that not only improved the compromise between alignment magnitude and spectral resolution, but also permitted measurement of residual dipolar couplings in a much broader range of systems awaited the work by Bax and Tjandra. In 1997, they showed that by going back to a dilute liquid crystalline medium a ten-fold increase in macromolecular alignment (relative to paramagnetic alignment) could be achieved without any sacrifice in spectral resolution (Tjandra & Bax, 1997a). Residual dipolar coupling contributions to ^{15}N–^{1}H splittings measured in ubiquitin were as large as 20 Hz, and could be measured with a precision of approximately 0·2 Hz. This corresponds to the determination of an internuclear vector orientation with an accuracy ranging between 0·5 and 5 degrees; an astonishing level of accuracy. The medium used was a dilute 'bicelle' medium,

which is based on an aqueous dispersion of lipid bilayer disks (Ram & Prestegard, 1988; Sanders & Schwonek, 1992). It proved compatible with proteins and other biomolecules, and it proved amenable to adjustment for ideal levels of alignment. The last barrier to widespread macromolecular application was thus overcome. Much of what we will discuss herein concerns the rapid progress that has been made in just a few years since this last significant step.

2. Theoretical treatment of dipolar interactions

2.1 Anisotropic interactions as probes of macromolecular structure and dynamics

The collection of NMR data in media that allow the measurement of many types of residual representations of tensorial interactions clearly can provide additional information about the structure of macromolecules. Interpretation of these residual tensorial interactions, however, is complicated because the information is a convolution of structural and dynamic contributions (Prestegard, 1998; Tolman *et al*. 1997). In this section, we discuss the sensitivity of residual interactions to both structural and dynamic molecular properties, and the means of deconvoluting these contributions. Although we restrict the discussion specifically to a treatment of the dipolar interaction, the results can easily be generalized to apply to other residual second rank interactions, such as anisotropic chemical shifts or quadrupolar interactions, as they depend on the same spatial functions. We employ a spherical representation of these angular functions because of their convenient rotational transformation properties. Nevertheless, we do at times draw comparisons with Cartesian representations, which are more convenient for physical interpretation.

2.1.1 The dipolar interaction

For a weakly coupled pair of spins, i and j, the dipolar contribution to the observed resonance splitting can be simply related to the expectation values of the dipolar Hamiltonian for the four product states, $\alpha\alpha$, $\alpha\beta$, $\beta\alpha$, $\beta\beta$ (Ernst *et al*. 1987),

$$D_{ij}^{\mathrm{res}} = \langle H_{ij}^{D}\rangle_{\beta\beta} - \langle H_{ij}^{D}\rangle_{\beta\alpha} - \langle H_{ij}^{D}\rangle_{\alpha\beta} + \langle H_{ij}^{D}\rangle_{\alpha\alpha}. \tag{1}$$

In the high field limit, it is a very good approximation to neglect all but the secular part of the dipolar Hamiltonian. Thus, we consider only a truncated dipolar Hamiltonian expressed in the lab frame (units of Hz),

$$H_{ij}^{D}(t) = -\left(\frac{\mu_0}{4\pi}\right)\frac{\gamma_i \gamma_j \hbar}{2\pi^2 r_{ij}^3} I_{iz} I_{jz} \mathrm{P}_2(\cos\theta(t)), \tag{2}$$

where r_{ij} is the internuclear distance between spins, γ_i and γ_j are the gyromagnetic ratios of spins i and j, and I_{kz} are spin angular momentum operators. The angular portion of the dipolar Hamiltonian is described using the second rank Legendre function, $\mathrm{P}_2(\cos\theta(t))$, which is a function of the angle θ subtending the magnetic field and the ijth internuclear vector. As we will show, the expectation value of the dipolar Hamiltonian does not vanish

https://doi.org/10.1017/S0033583500003656 Published online by Cambridge University Press

in ordered systems. Indeed, the residual interaction observed in these cases contains a wealth of information pertaining to molecular structure and dynamics.

2.1.2 Averaging in the solution state

In the solution state, the time dependence of the dipolar Hamiltonian arises from several sources. These include fluctuations in the internuclear distance as well as reorientation of the internuclear vector due to overall molecular reorientation and internal motions. Measured residual dipolar couplings are the time-averaged resultant of these processes, denoted by angle brackets,

$$D_{ij}^{\mathrm{res}} = -\left(\frac{\mu_0}{4\pi}\right)\frac{\gamma_i \gamma_j h}{2\pi^2}\left\langle \frac{\mathrm{P}_2(\cos\theta(t))}{r_{ij}^3}\right\rangle. \tag{3}$$

This can be simplified further by recognizing that local bond librations and other motions are likely to occur on very different timescales, and thus their averages can be computed independently. The use of an effective internuclear distance allows the elimination of an explicit consideration of the effects of bond librations,

$$D_{ij}^{\mathrm{res}} = -\left(\frac{\mu_0}{4\pi}\right)\frac{\gamma_i \gamma_j h}{2\pi^2 r_{ij,\mathrm{eff}}^3}\langle \mathrm{P}_2(\cos\theta(t))\rangle. \tag{4}$$

Henceforth it will be implicitly assumed that r refers to the appropriate effective internuclear distance. As noted by Case (Case, 1999), this effective internuclear distance is likely to be longer than the mean internuclear distance. Once local bond motions are removed, the average of the angular part reflects the orientational distribution of the effective ij internuclear vector relative to the magnetic field. Under an isotropic distribution of molecular orientations this average will vanish, explaining why dipolar couplings are not typically observed in high resolution NMR. Even under anisotropic distributions, however, the above expression is still of little practical use because the angular average that appears is a convolution of the effects of overall molecular motion, segmental internal motions, and structural characteristics. We focus our attention on the separation of these effects.

2.2 Ordering of a rigid body

The problem is considerably more tractable if one treats the molecule (or molecular fragment) as a rigid body containing a number of dipolar interaction vectors with known geometric relationships one to another. Choice of an arbitrary reference coordinate system, that is fixed within the molecule, allows description of the orientation of the ijth internuclear vector in terms of its time independent polar angles θ and ϕ. Likewise, at any instant in time, the orientation of the magnetic field can be described in terms of its polar angles $\zeta(t)$ and $\xi(t)$, which are time dependent due to overall reorientation of the molecule. The situation is diagrammed in Fig. 1. The $\mathrm{P}_2(\cos\theta(t))$ term is thus expanded making use of the spherical harmonic addition theorem,

$$\mathrm{P}_2(\cos\theta(t)) = \frac{4\pi}{5}\sum_{q=-2}^{2} Y_{2q}^{*}(\theta\phi)\, Y_{2q}(\zeta(t)\,\xi(t)), \tag{5}$$

https://doi.org/10.1017/S0033583500003656 Published online by Cambridge University Press

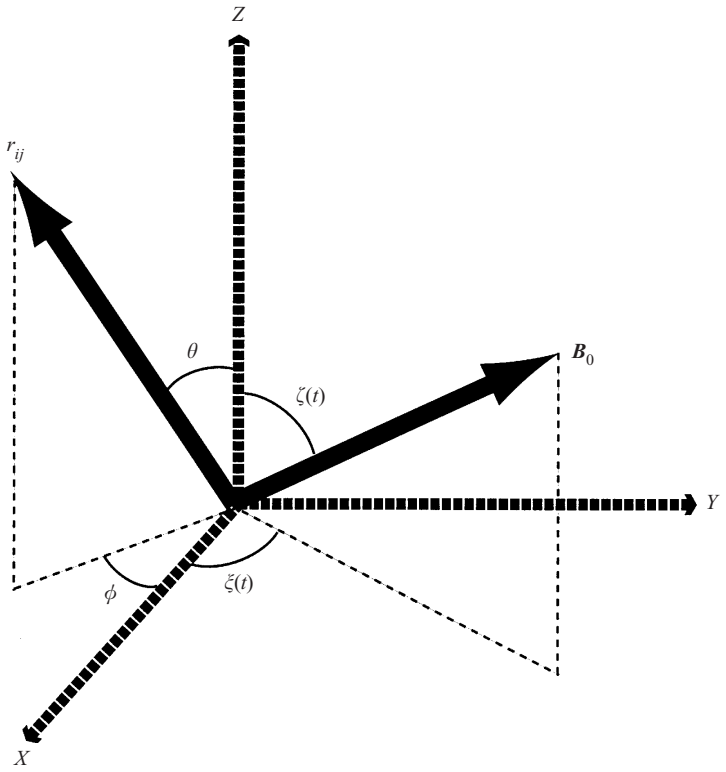

Fig. 1. Depiction of the orientation of the internuclear vector and the magnetic field relative to a molecule fixed frame. The time dependence of the magnetic field vector arises due to molecular reorientation.

where the *Y*s refer to the normalized spherical harmonics. Inserting equation (5) into equation (4) leads to the following expression for the residual dipolar coupling,

$$D_{ij}^{\text{res}} = -\left(\frac{\mu_0}{4\pi}\right)\frac{\gamma_i \gamma_j h}{2\pi^2 r_{ij}^3}\frac{4\pi}{5}\sum_{q=-2}^{2} Y_{2q}^{*}(\boldsymbol{\Phi}) \langle Y_{2q}(\boldsymbol{\Omega}(t))\rangle. \tag{6}$$

where $\boldsymbol{\Phi} = (\theta, \phi)$ and $\boldsymbol{\Omega}(t) = (\zeta(t), \xi(t))$ have been used to represent the polar angles of the internuclear vector and the magnetic field relative to the molecule fixed frame, respectively. Note that the assumption of molecular rigidity allows the angular time dependence to be easily factored entirely into just one set of angles ($\boldsymbol{\Omega}(t)$).

2.2.1 The Saupe order tensor

It is clear that, when combined with a knowledge of the structure of the molecule or molecular fragment, measurement of dipolar couplings corresponding to at least five independent dipolar interaction vectors will allow all five averages appearing in equation (6) to be determined. This procedure corresponds to a determination of Saupe's order tensor, originally formulated in a Cartesian representation similar to the following (Saupe, 1968):

$$D_{ij}^{\text{res}} = -\left(\frac{\mu_0}{4\pi}\right)\frac{\gamma_i \gamma_j h}{2\pi^2 r_{ij}^3}\sum_{kl} S_{kl}\cos(\alpha_k)\cos(\alpha_l). \tag{7}$$

https://doi.org/10.1017/S0033583500003656 Published online by Cambridge University Press

Here, the internal geometry is represented by direction cosines describing the orientation of the internuclear vector within the molecular frame. Overall motion and orientation of the alignment frame is absorbed into the elements S_{kl}, which form the order tensor, a traceless, symmetric 3×3 matrix having just five independent elements. The Cartesian and spherical representations are related by the following linear transformations:

$$\left.\begin{aligned}
S_{xz} &= \sqrt{\frac{3}{8}}\sqrt{\frac{4\pi}{5}}(\langle Y_{21}(\Omega(t))\rangle - \langle Y_{2-1}(\Omega(t))\rangle) \\
S_{yz} &= i\sqrt{\frac{3}{8}}\sqrt{\frac{4\pi}{5}}(\langle Y_{2-1}(\Omega(t))\rangle + \langle Y_{21}(\Omega(t))\rangle) \\
S_{xy} &= i\sqrt{\frac{3}{8}}\sqrt{\frac{4\pi}{5}}(\langle Y_{22}(\Omega(t))\rangle - \langle Y_{2-2}(\Omega(t))\rangle) \\
S_{xx} - S_{yy} &= \sqrt{\frac{3}{2}}\sqrt{\frac{4\pi}{5}}(\langle Y_{22}(\Omega(t))\rangle + \langle Y_{2-2}(\Omega(t))\rangle) \\
S_{zz} &= \sqrt{\frac{4\pi}{5}}\langle Y_{20}(\Omega(t))\rangle.
\end{aligned}\right\} \tag{8}$$

The extraction of molecular orientation information from order information contained in the above expressions is achieved by diagonalization of the order tensor. The principle values can be recast into an order parameter for the most ordered axis, S_{zz}, and an asymmetry parameter, $\eta = (S_{xx} - S_{yy})/S_{zz}$, which describes the deviation from axially symmetric ordering. The transformation leading to diagonalization also relates the orientation of the principal alignment axes to the initial molecular frame, and hence, describes the mean orientation of the molecule, or a fragment of the molecule, relative to the magnetic field. This transformation is frequently represented in terms of three Euler angles. In Section 5 we will discuss briefly how this transformation can be used to generate a molecular structure by rotating fragments to a common alignment frame. Here, we will maintain our focus on the nature of the averaging process.

Working in the principal axis frame described by the three Euler angles, only two of the averages in equation (6) remain nonzero. These two averages can also be related to the anisotropies of a generalized alignment tensor (Tjandra & Bax, 1997b), as well as to elements of the Saupe order tensor,

$$\left.\begin{aligned}
\langle Y_{20}(\Omega(t))\rangle &= \sqrt{\frac{5}{4\pi}}S_{zz} = \sqrt{\frac{5}{4\pi}}A_{\mathrm{a}} \\
\langle Y_{2\pm2}(\Omega(t))\rangle &= \sqrt{\frac{5}{24\pi}}(S_{zz} - S_{yy}) = \sqrt{\frac{15}{32\pi}}A_{\mathrm{r}}.
\end{aligned}\right\} \tag{9}$$

For cases in which alignment is achieved due to interaction between the magnetic field and the anisotropic magnetic susceptibility of the molecule, an analytical description of the

https://doi.org/10.1017/S0033583500003656 Published online by Cambridge University Press

magnitudes of overall alignment can be formulated, provided that solute molecules do not interact with one another. This has been discussed previously (Prestegard *et al*. 1999). For convenience, we cite the relevant expressions for the generalized overall alignment anisotropies in terms of magnetic susceptibility anisotropies (units of m^3),

$$\mathcal{A}_a = \Delta\chi\left[\frac{B^2}{15\mu_0 kT}\right], \quad \mathcal{A}_r = \delta\chi\left[\frac{B^2}{15\mu_0 kT}\right]. \tag{10}$$

2.2.2 Orientational probability distribution function

The parameters of the Saupe order tensor are very closely related to the probability distribution function describing the orientation of a rigid body relative to a reference vector (Snyder, 1965); in this case the molecule (or molecular fragment) relative to the magnetic field. More specifically, determination of the Saupe order tensor parameters provides a full description of the second rank part of the orientational probability distribution function (OPDF). To see this, we consider a general expression for this probability distribution function as an infinite series of spherical harmonics,

$$\mathrm{P}(\theta\phi) = \frac{1}{4\pi} + \sum_{l=1}^{\infty}\sum_{m=-l}^{l} c_{lm}\, Y^*_{lm}(\theta\phi), \tag{11}$$

where θ and ϕ are the polar angles describing the orientation of the reference vector relative to a molecule fixed set of coordinate axes, the Ys are the normalized spherical harmonics, and the cs are scalar coefficients. In general, an infinite number of coefficients are required to fully describe this OPDF. The necessary time averages in equation (6) are easily computed making use of the orthogonality of the spherical harmonics.

$$\langle Y_{2q}(\zeta(t)\,\xi(t))\rangle = \int\int \mathrm{P}(\theta\phi)\, Y_{2q}(\theta\phi)\sin\theta d\theta d\phi = c_{lm}\,\delta_{2l}\,\delta_{mq} = c_{2q}. \tag{12}$$

The fact that the dipolar interaction is a second rank interaction means that only knowledge of the five coefficients for the second rank part of the OPDF is necessary in order to predict the residual dipolar couplings observed for a rigidly reorienting body. A detailed knowledge of all the molecular interactions that lead to alignment is not strictly necessary for an analysis of residual dipolar couplings.

2.2.3 The generalized degree of order

It is useful to have a simple scalar parameter that reflects the overall degree of ordering. S_{zz} serves this purpose for axially symmetric systems, but it is not the best overall measure of order in axially asymmetric cases. If we consider the averaged spherical harmonics in equation (6) as a 5-vector (Moltke & Grzesiek, 1999), then such a parameter can be defined as the Euclidean norm of this vector. We refer to this parameter, ϑ, as the generalized degree of order (GDO) (Tolman *et al*. personal communication). It is easily derived from the spherical or Cartesian (order tensor) representations,

$$\vartheta = \sqrt{\frac{4\pi}{5}\sum_k \overline{|\langle Y_{2k}(\Omega(t))\rangle|^2}} = \sqrt{\frac{2}{3}\sum_{ij}\overline{S_{ij}^2}}. \tag{13}$$

Interestingly, for sufficiently large and random distributions of dipolar interaction vector

https://doi.org/10.1017/S0033583500003656 Published online by Cambridge University Press

orientations, ϑ can also be obtained from the standard deviation of the observed residual dipolar coupling distribution,

$$\sigma_{D^{\mathrm{res}}} = \sqrt{\frac{1}{5}}\left|\left(\frac{\mu_0}{4\pi}\right)\frac{\gamma_i\gamma_j\hbar}{2\pi^2 r_{ij}^3}\right|\vartheta. \tag{14}$$

The GDO is a potentially useful parameter because it does not depend on the spatial coordinates of the system; it is exclusively sensitive to dynamic properties, whether arising from overall magnitude of alignment or from internal motions.

2.3 Molecular structure and internal dynamics

Thus far we have discussed the determination of the order tensor for a molecule, or molecular fragment, assuming that its internal structure is known and is well represented by a single rigid entity. The presence of internal motions complicates the situation (Tolman *et al*. 1997). Both structural and motional variation affect measured residual dipolar couplings, and, in general, the effects must be separated before conclusions about either structure or internal motion can be drawn. In certain situations, where motional amplitudes are large and correlated with overall alignment, this separation will be a complicated process, requiring a great deal of additional experimental information. However, provided that these motions are uncorrelated with overall molecular alignment, one can reformulate expressions for dipolar coupling in terms of a mean interaction vector orientation and a small set of parameters describing the extent and principal direction of internal motion. Referring back to equation (6), one can write an expression for residual dipolar couplings, as a scalar contraction over separate angular averages for overall and internal motion. Note that this partitioning requires the choice of some arbitrary molecule fixed frame. This is most easily accomplished for cases in which internal motions are not too large, or when overall alignment is dominated by some well structured region of the molecule. For simplicity, we specify here that this frame correspond to the PAS of overall alignment.

$$D_{ij}^{\mathrm{res}} = -\left(\frac{\mu_0}{4\pi}\right)\frac{\gamma_i\gamma_j\hbar}{2\pi^2 r_{ij}^3}\frac{4\pi}{5}\sum_q \langle Y_{2q}^*(\theta(t)\,\phi(t))\rangle\,\langle Y_{2q}(\zeta(t)\,\xi(t))\rangle\,. \tag{15}$$

An explicit separation of internal averaging and mean orientation can now be obtained by transformation into a principal axis system for the interaction vector. In this frame, the z-axis corresponds to the mean orientation of the interaction vector while the orientation of the x-axis depends on the spatial nature of internal motion involving that vector. This is illustrated in Fig. 2. We note that in general, characterization of an elliptical averaging trajectory as shown in Fig. 2, represents the maximum amount of information that can be retrieved from dipolar coupling measurements alone. Computationally, defining this ellipse is quite analogous to finding the principal axes and values of overall alignment. We define the following transformation,

$$\langle Y_{2q}(\theta(t)\,\phi(t))\rangle = \sum_{q'}\langle Y_{2q'}(\theta'(t)\,\phi'(t))\rangle\, D_{q'q}^{(2)}(\phi_{\mathrm{av}}\,\theta_{\mathrm{av}}\,\psi), \tag{16}$$

where the $D_{qq'}^{(2)}$ represent Wigner rotation matrix elements for the transformation from the overall alignment frame to the interaction PAS. The angles θ_{av} and ϕ_{av} correspond to the polar angles describing the mean orientation of the interaction vector within the overall

https://doi.org/10.1017/S0033583500003656 Published online by Cambridge University Press

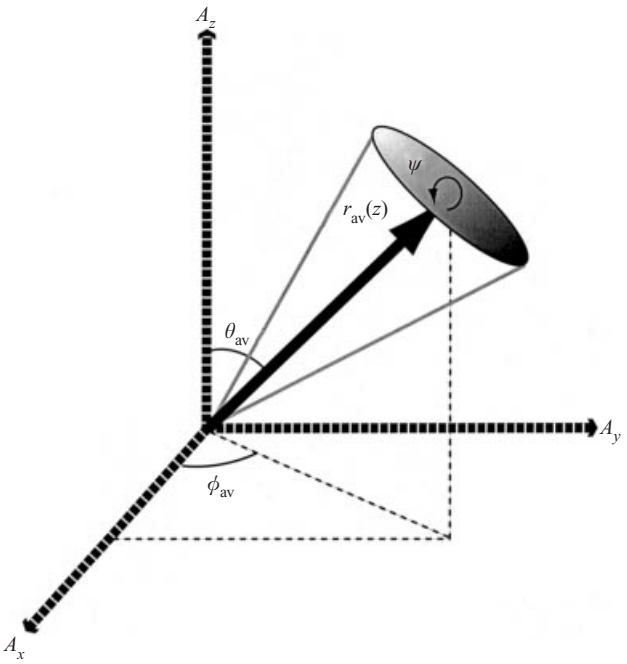

Fig. 2. Relative to the principal axes of overall molecular alignment (A_x, A_y, A_z), the orientation of the interaction principal axis system is described by the three Euler angles (θ_{av}, ϕ_{av}, ψ). Note that θ_{av} and ϕ_{av} describe the mean vector orientation and the angle ψ is necessary to properly orient the principle direction of motional anisotropy, if present.

alignment frame. The angle ψ describes the principle direction of anisotropy of internal motion of the vector, corresponding to the orientation of the x-axis of the interaction PAS illustrated in Fig. 2. Substitution of the above into equation (15) leads to,

$$D_{ij}^{\text{res}} = -\left(\frac{\mu_0}{4\pi}\right)\frac{\gamma_i\gamma_j\hbar}{2\pi^2 r_{ij}^3}\frac{4\pi}{5}\sum_{qq'}\langle Y_{2q'}((-\phi(t))\rangle D_{qq'}^{(2)}(-\psi-\theta_{av}-\phi_{av})\langle Y_{2q}(\Omega(t))\rangle, \tag{17}$$

where $\Phi(t) = (\theta'(t), \phi'(t))$ and $\Omega(t) = (\zeta(t), \xi(t))$ have been used to represent the polar angles of the internuclear vector and the magnetic field relative to the interaction and overall alignment principal axis frames, respectively. Expressed in their respective PASs, these averages have a particularly simple representation. As discussed earlier (equation (9)), the averages $\langle Y(\Omega(t)\rangle$ are identified with overall alignment. On the other hand, the averages $\langle Y(\Phi(t)\rangle$ can be related to a pair of order parameters describing the extent of internal motion of the specific interaction vector,

$$\sqrt{\frac{4\pi}{5}}\langle Y_{20}(\Omega(t))\rangle = S_{zz,\text{int}}, \quad \sqrt{\frac{24\pi}{5}}\langle Y_{2\pm2}(\Phi(t))\rangle = (S_{xx,\text{int}} - S_{yy,\text{int}}). \tag{18}$$

As defined, the order parameters correspond to the following averages computed within the interaction PAS,

$$S_{zz,\text{int}} = \langle\tfrac{1}{2}(3\cos^2\theta'(t)-1)\rangle, \quad (S_{xx,\text{int}} - S_{yy,\text{int}}) = \langle\tfrac{3}{2}\sin^2\theta'(t)\cos 2\phi'(t)\rangle. \tag{19}$$

Making these substitutions and expanding equation (17) leads to a more generally applicable

https://doi.org/10.1017/S0033583500003656 Published online by Cambridge University Press

expression for the residual dipolar coupling in an aligned molecule. In the case where the molecular frame is assumed to coincide with the overall alignment frame the expression is as follows.

$$D_{ij}^{\mathrm{res}} = -\left(\frac{\mu_0}{4\pi}\right)\frac{\gamma_i \gamma_j h}{2\pi^2 r_{ij}^3}\{S_{zz,\mathrm{int}}[S_{zz}\tfrac{1}{2}(3\cos^2\theta_{\mathrm{av}}-1)+\tfrac{1}{2}(S_{xx}-S_{yy})\sin^2\theta_{\mathrm{av}}\cos 2\phi_{\mathrm{av}}]$$
$$+\tfrac{1}{2}(S_{xx,\mathrm{int}}-S_{yy,\mathrm{int}})\,[\tfrac{1}{2}S_{zz}\sin^2\theta_{\mathrm{av}}\cos 2\psi$$
$$+\tfrac{1}{3}(S_{xx}-S_{yy})\,(\cos 2\psi\cos 2\phi_{\mathrm{av}}(\tfrac{3}{4}+\tfrac{1}{4}\cos 2\theta_{\mathrm{av}})-\sin 2\psi\sin 2\phi_{\mathrm{av}}\cos\theta_{\mathrm{av}})]\}. \quad (20)$$

In the limit that internal motion is axially symmetric about the vector mean orientation, the above equation can be simplified to the following:

$$D_{ij}^{\mathrm{res}} = -\left(\frac{\mu_0}{4\pi}\right)\frac{\gamma_i \gamma_j h}{2\pi^2 r_{ij}^3} S_{zz,\mathrm{int}}\{\tfrac{1}{2}S_{zz}(3\cos^2\theta_{\mathrm{av}}-1)+\tfrac{1}{2}(S_{xx}-S_{yy})\sin^2\theta_{\mathrm{av}}\cos(2\phi_{\mathrm{av}})\}. \quad (21)$$

The parameters describing internal motion in equations (20) and (21) bear a relationship to parameters typically extracted from NMR spin relaxation data. $S_{zz,\mathrm{int}}$ corresponds mathematically to the spin relaxation order parameter, but exhibiting a sensitivity to motions extending to the millisecond timescale. For motions which are not axially symmetric, the mathematical relationship of these dipolar 'order parameters' to the generalized order parameter, S, used in spin relaxation studies can be established by consideration of equation (19).

$$S^2 = S_{zz,\mathrm{int}}^2+\tfrac{1}{3}(S_{xx,\mathrm{int}}-S_{yy,\mathrm{int}})^2. \quad (22)$$

In general, the complexity of the motion that can be described is limited by the nature of the residual dipolar measurements and can be reduced to a depiction as an ellipse similar to that shown in Fig 2.

The key to producing both simplified equations (20) and (21) is an assumption that internal motion does not lead to a set of conformers that each exhibits different overall alignment properties. In other words, this approach is designed for cases where internal motions are not so large as to make the concept of a single mean structure ambiguous. This is certainly likely to hold for many macromolecular applications of interest, and is important to our ability to determine structure of biomolecules in the presence of modest levels of internal motion.

3. Inducing molecular order in high resolution NMR

3.1 Tensorial interactions between the magnetic field and anisotropic magnetic susceptibilities

To date, most high resolution NMR applications in partially ordered systems have relied either directly or indirectly on the interaction between the magnetic field and a molecule's magnetic susceptibility anisotropy in order to achieve the desired alignment. Upon placement of a molecule in a magnetic field, a magnetic dipole moment is induced which is proportional to the susceptibility, χ. For diamagnetic molecules ($\chi < 0$), induced moments will oppose the field while for paramagnetic molecules ($\chi > 0$), induced moments will be along the field (Van Vleck, 1932). These induced moments will in turn interact with the magnetic field. Molecules

https://doi.org/10.1017/S0033583500003656 Published online by Cambridge University Press

of non-spherical symmetry will exhibit an orientational dependence of this interaction due to their anisotropic distribution of electron density. Thus, the susceptibility is a tensorial quantity and the orientation dependent energy of interaction, W, can be written as follows (Bastiaan *et al*. 1987),

$$W = \frac{1}{\mu_0}(-\tfrac{1}{2}\boldsymbol{B}\cdot\boldsymbol{\chi}\cdot\boldsymbol{B}). \tag{23}$$

The size of the interaction energy (W) depends on the square of the magnetic field strength ($\boldsymbol{B}^2$) and the magnetic susceptibility tensor, $\boldsymbol{\chi}$. Variations in W with orientation arise from the anisotropic part of the $\boldsymbol{\chi}$ tensor, and if these variations are large enough compared to the thermal energy, kT, a measurable degree of orientational order will be induced.

For the purpose of measuring residual dipolar interactions in macromolecules, field induced orientation is achieved using one of two fundamental approaches. Macromolecules can be dissolved in cooperatively aligned media, where they physically interact with elements of the media, or macromolecules can be directly aligned if they have sufficiently large susceptibility anisotropies of their own. There are also new approaches that share aspects of each. For example, two groups have used specific interactions with fragments of purple membrane from photosynthetic bacteria to orient solutes (Koenig *et al*. 1999; Sass *et al*. 1999). The fragments have sufficient susceptibility anisotropy to align independently, but a physical interaction is used to align a molecule of interest. There are advantages associated with each fundamental approach. Cooperatively aligned media are generally applicable to the widest range of systems. Moreover, the degree of solute alignment is usually higher and often tunable. Direct magnetic field alignment, on the other hand, often allows independent determination of the degree of alignment, and thus, may become the method of choice for binding or dynamics studies. In what follows, we describe developments in these two important areas.

3.2 Dilute liquid crystal media: a tunable source of order

At this point in time, a whole array of liquid crystalline solvent systems useful for inducing molecular alignment of macromolecules, have been introduced (Sanders *et al*. 1994; Clore *et al*. 1998d; Hansen *et al*. 1998; Prosser *et al*. 1998a; Koenig *et al*. 1999; Sass *et al*. 1999; Barrientos *et al*. 2000). These have greatly enhanced the possibility of finding a medium compatible with the maintenance of native macromolecule structure and function. Here, we focus our discussion on the two aligning media most commonly used in high-resolution applications: the initial disc-shaped bicelles and the more recently introduced filamentous bacteriophage. In Fig. 3, the structures of these ordered particles are depicted (Sanders *et al*. 1994; Clore *et al*. 1998d; Hansen *et al*. 1998). Both of these solvent systems are highly ordered under the influence of a moderate magnetic field and usually transmit this order to solute molecules by nonspecific collisional or electrostatic interactions. Using these media, the alignment of solute molecules is tunable simply by increasing or decreasing the concentration of the order inducing component (Tjandra & Bax, 1997a). In general, a solute alignment of 0·1% is readily attainable (Tjandra, 1999), providing an excellent compromise between the magnitude of desired residuals, and the maintenance of spectral resolution.

The alignment of particles comprising liquid crystal media can conveniently be probed by using deuterated solvents and by observing the quadrupolar splitting of the deuterium

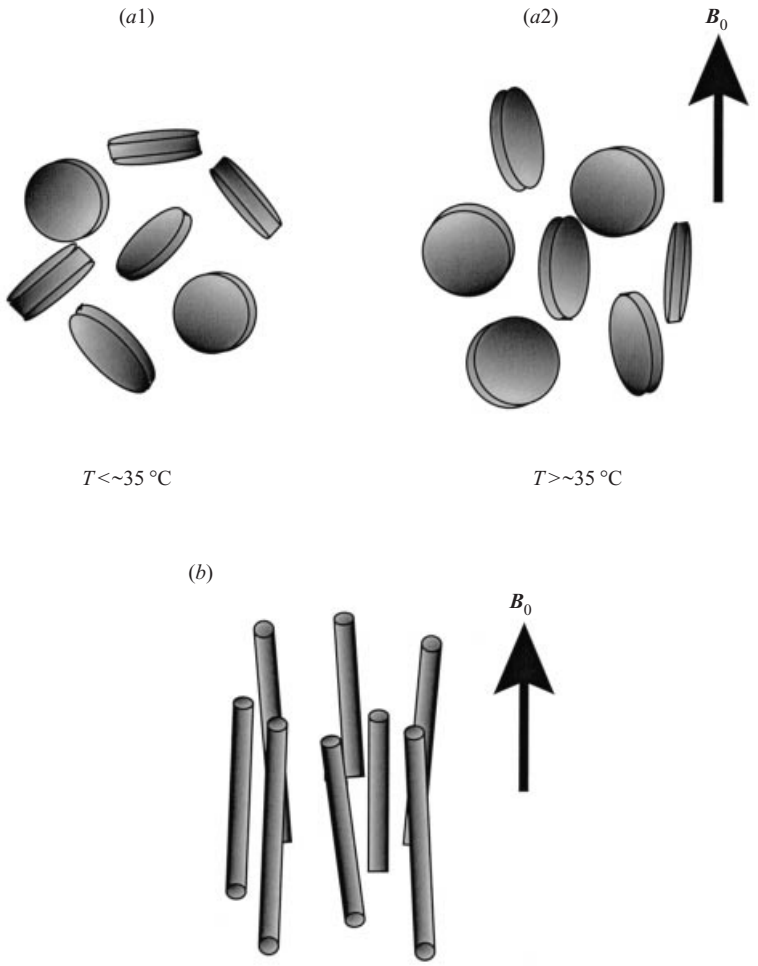

Fig. 3. Liquid crystal media used in aligning biomolecules. (*a*) Bicelles are believed to be disc-shaped pieces of lipid bilayers, at least under conditions of their initial characterization. (*a* 1) At temperatures < 35 °C, bicelles oriented isotropically in solution. (*a* 2) At temperatures > 35 °C, bicelles undergo a phase transition and align with their bilayer normal perpendicular to the applied magnetic field. (*b*) Filamentous phage are rod-like particles that are believed to align with their long axis parallel to the field.

resonance that results from incomplete averaging of the quadrupolar interaction. The order induced in the solvent is likely due to exchange between bulk solution and the solvation shell of the ordered particles. In Fig. 4, we show an example of a 1D ^{2}H spectrum acquired on a homogenous and well behaved bicelle solution in the liquid crystalline phase.

3.2.1 Bicelles: from membrane mimics to aligning media

Bicelles have thus far been the most widely used aligning media in high resolution NMR applications (Sanders & Prosser, 1998). Much of what is known about the physical properties of bicelles comes from their original use as membrane mimics in solid state studies of membrane associated molecules (Ram & Prestegard, 1988; Sanders & Prestegard, 1990;

https://doi.org/10.1017/S0033583500003656 Published online by Cambridge University Press

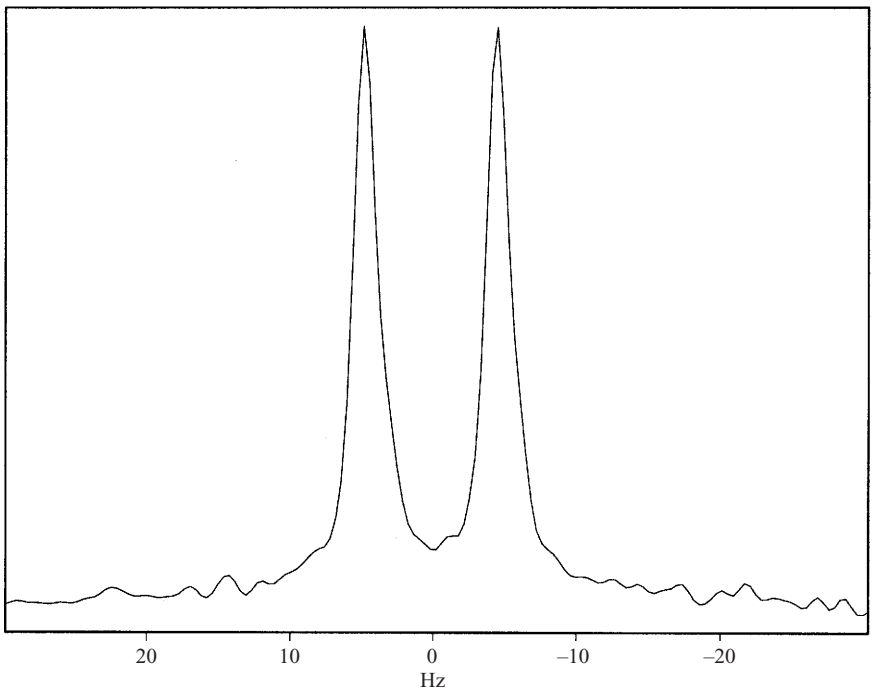

Fig. 4. ^{2}H 1D spectrum of water deuterons in a 5% bicelle prepared in D_2O at 35 °C. The size of the splitting is ~ 10 Hz and increases almost linearly with bicelle concentration. The presence of two well resolved and equally intense doublets suggests that the sample is homogenous.

Sanders *et al*. 1994). These earlier applications typically used a high concentration of bicelles (> 20%) in aqueous buffer, with the bicelles composed of mixtures of dimyristoyl-phosphatidylcholine (DMPC) with either dihexanoyl-phosphatidylcholine (DHPC) or the bile salt derivative, 3-(cholamidopropyl)dimethylammonio-2-hydroxy-1-propane-sulfonate (CHAPSO). Under the limited set of concentration and composition conditions, investigated bicelles have been characterized as disc-shaped assemblies, several hundreds of angstroms (200–250 Å) in diameter and ~ 40Å in thickness (Fig. 3(*a*)) (Chung & Prestegard, 1993; Hare *et al*. 1995). DMPC is believed to make up the bulk of the plane of the disc, while the shorter detergent stabilizes the edges. These bicelles cooperatively align with their normal perpendicular to the magnetic field, and adopt a nematic liquid crystalline phase. Both the number of lipids in the bicelle and the cooperative alignment of bicelles in the liquid crystal domain amplify the magnitude of the anisotropy tensor and result in very high levels of order, even at moderate field strengths (Sanders & Prosser, 1998). Ordered bicelle domains exist only over well-defined limits of composition, temperature, and presumably pressure (Sanders *et al*. 1994; Sanders & Prosser, 1998). While boundaries of the phase diagram describing conditions under which bicelles order have not been fully investigated, a very useful transition occurs as the temperature is lowered below 25 °C for DMPC based systems (Fig. 3(*a*)). An isotropic phase, presumably composed of smaller, thicker and less anisotropic particles is formed. This proves useful in that an isotropic reference spectrum can be collected on the same sample by simply lowering temperature. This is often essential because splittings are frequently the sum of scalar and dipolar couplings, and must be separated by measuring the scalar component in an isotropic phase (Tjandra & Bax, 1997a).

https://doi.org/10.1017/S0033583500003656 Published online by Cambridge University Press

In order to retain the spectral simplicity and resolution needed for high resolution NMR applications, dilution of bicelle media to 3%–10% (w/v) is usually necessary (Tjandra & Bax, 1997a). At these lower concentrations, bicelle formation occurs over a narrower ratio of DHPC:DMPC (2·9–3·7) and narrower temperature range of (35–42 °C) (Ottiger & Bax, 1998; Tjandra & Bax, 1997a). At such concentrations, bicelles still cooperatively align despite the fact that the average spacing between bicelles exceeds 400 Å at 5% (Bax & Tjandra, 1997). It appears likely that bicelles become larger at these lower concentrations, as more short chain lipid molecules partition into the buffer solution (Ottiger & Bax, 1998). In fact, some good correlations of lipid ratios with such physical properties have been established (Vold & Prosser, 1996). The large inter bicelle space at low concentrations is important. Under these conditions, the rotational diffusion of biomolecules is almost unaffected by the presence of the bicelle particles, thereby preserving the quality of high resolution NMR spectra (Ottiger & Bax, 1998; Tjandra & Bax, 1997a).

Some of the key limitations of the original bicelle media are lack of tolerance to a wide range of biologically relevant conditions, and a limited life span (Ottiger & Bax, 1998; Sanders & Prosser, 1998). In applications to charged solutes, bicelles can be stabilized by doping with similarly charged amphiphiles, thus reducing the risk of precipitation or phase separation (Losonczi & Prestegard, 1998a). It has also been shown that the longevity of the original, hydrolysis-prone, ester based bicelles can be extended using an ether based bicelle system (Cavagnero *et al*. 1999; Ottiger & Bax, 1999); this modification also increases the tolerance of bicelle systems to harsh pH conditions. Other innovations in bicelle design include modifications to allow studies at lower temperatures (Wang *et al*. 1998a), and modification of the basic orientational properties of bicelle media by doping with certain lanthanide ions to cause bicelles to orient with their normal parallel to the applied magnetic field (Prosser *et al*. 1996). Recently, a lanthanide-carrying phospholipid chelate has been introduced as a lipid bilayer component, which minimizes line-broadening effects in cases where molecules of interest are strongly associated with bicelles (Prosser *et al*. 1998b). We expect that the applicability of bicelle media to a variety of protein, DNA and carbohydrate systems will continue to increase as their design evolves.

3.2.2 Filamentous phage

Soon after the introduction of dilute bicelles, it was shown that phage or viral particles could constitute an effective alignment medium (Clore *et al*. 1998d; Hansen *et al*. 1998). Here we focus our discussion on bacteriophage Pf1, since it has been the most extensively studied and described (Hansen *et al*. 1998, 2000). Bacteriophage Pf1 consists of a single stranded circular DNA genome that is packaged in coat protein at a nucleotide to coat protein ratio of approximately 1:1. This packaging forms a rod approximately 60 Å in diameter and approximately 20,000 Å in length, which orients with its long axis parallel to the field (Fig. 3(*b*)). Some advantages of phage media are that it is extraordinarily stable to different conditions in solution, and unlike the bicelle medium, the ordered phase exists over a wide temperature range (5–> 45 °C). Moreover, the phage fully aligns over a very wide range of phage concentration. This is perhaps not surprising, given the large dimensions of the phage particles, and the possibility that even non-cooperative, single particle alignment helps extend alignment to lower concentrations.

Pf1 appears particularly well suited for studies of nucleic acids. Since Pf1 is negatively charged at physiological pH (pI = 4·0), the negatively charged nucleic acid molecules will not bind to the phage particle, thereby preventing unfavorably high levels of alignment or sample aggregation (Hansen *et al*. 1998). The high negative charge and inability to vary the charge does exclude many applications to positively charged macromolecules. One other disadvantage is that two NMR samples are usually needed, one with, and one without, phage media, in order to separate isotropic J values from the sum of isotropic J values and residual dipolar couplings. Notably, in a recent application, magic angle spinning has been used to produce a pseudo isotropic condition (A. Pardi, personal communication, 2000).

3.2.3 Transfer of alignment from ordered media to macromolecules

Understanding the mechanism by which order is transferred to the solute molecules from the aligning medium is an important issue. It has fundamental implications for tuning of the level of alignment, improving stability, and, potentially, selecting information on bound states. Also, the ability to vary the nature of solute alignment can be a powerful aid to structure determination.

For most biomolecules dissolved in orienting media, the mechanism of alignment must rely on weak interactions because order must be induced without distorting the molecule or sacrificing high resolution. The dominance of weak interactions in most applications is supported by the fact that orienting media do not lead to changes in observed biomolecule chemical shifts, indicating that interactions do not cause any measurable structural perturbations (note that small departures in chemical shift $< 0{\cdot}1$ p.p.m. for ^{15}N and ^{13}C and $< 0{\cdot}01$ p.p.m. for ^{1}H, can be expected due to incomplete averaging of the chemical shift anisotropy) (Bax & Tjandra, 1997; Ottiger & Bax, 1998). The absence of significant structural deviations is also substantiated by the close agreement between measured residual dipolar couplings and values predicted based on structural models determined by traditional NMR methods or X-ray crystallography (Tjandra & Bax, 1997a). The absence of large effects is perhaps not surprising when one considers that departure from isotropy is often less than 1 in 1000, requiring energies that are a small fraction of kT.

It is becoming clear that molecular shape is an important factor in the alignment properties of a solute molecule. For many biomolecules dissolved in orienting media, the measured alignment tensor orientation is in near coincidence with orientation of the measured rotational diffusion tensor (de Alba *et al*. 1999). These observations led to the proposal of a collisional model for solute alignment (Bax & Tjandra, 1997; Tjandra & Bax, 1997a; de Alba *et al*. 1999; Tjandra, 1999). However, it is also clear that simple collisions are only one aspect of interaction, and that other factors can contribute to the transfer of order. It has, for example, been observed that doping bicelles with charged amphiphiles leads to changes in solute alignment properties (Ramirez & Bax, 1998), and substantially increased alignment and line broadening have been observed when oppositely charged aligning media and solutes are used (Koenig *et al*. 1999; Ojennus *et al*. 1999; Sass *et al*. 1999). For proteins with histidine tags, commonly used for protein purification purposes, variation in pH also leads to a difference in measured order tensor parameters (Ramirez & Bax, 1998). These observations suggest the presence of significant electrostatic contributions to solute alignment; a suggestion that is supported by the observation that effects are attenuated by increased ionic

strength (Sass *et al*. 1999). Charge variation, therefore, provides another experimental avenue for modulating and enhancing solute alignment; this will be important for obtaining an independent set of dipolar data (as will be discussed in Section 5).

3.3 Magnetic field alignment

For macromolecules having large magnetic susceptibility anisotropies direct magnetic field alignment is a reasonable alternative when very high magnetic fields are available. In practice, applications are limited to two general classes of macromolecules: (1) molecules with paramagnetic centers such as metalloproteins, and (2) regularly structured diamagnetic systems, such as DNA helices, where summation of individual group anisotropies can result in a significant net molecular anisotropy. Even for these systems, residual couplings are often one order of magnitude smaller than what is observed in ordered media, and small contributions to splittings such as dynamic frequency shifts and cross-correlation effects can become significant (Ghose & Prestegard, 1997). In most cases, residual dipolar contributions must also be measured as function of field strength to separate contributions of isotropic J couplings. There are, however, advantages. There is potentially useful additional information in the determination of native susceptibility tensors, and the ability to avoid the use of interacting media makes measurement using native alignment worthy of consideration. Moreover, the $\boldsymbol{B}^2$ dependence of alignment, does offer the possibility of more precise measurement as higher magnetic fields become available in the future.

3.3.1 Paramagnetic assisted alignment

Early application of paramagnetic assisted alignment employed native centers such as the iron containing heme of cyanometmyoglobin (Tolman *et al*. 1995). Similar applications on other paramagnetic proteins have appeared in the literature (Banci *et al*. 1998; Volkman *et al*. 1999; Demene *et al*. 2000). The domain of applicability of magnetic induced order, however, can be expanded by chemically imparting larger anisotropic magnetic susceptibilities to macromolecules. In most cases, this has involved the use of paramagnetic substitutes for native diamagnetic cations. Lanthanides, in particular, can impart a large paramagnetic anisotropy and, hence, greatly enhance levels of alignment. Harrocks and Sipe have compared anisotropies for the entire lanthanide series in 4-picoline adducts, $Ln(dpm)_3(4\text{-pic})_2$ (Horrocks & Sipe, 1972). This study shows that Dy^{3+} and Tb^{3+} are the lanthanide ions with the highest magnetic susceptibility anisotropy. However, in many cases, paramagnetic ions are unsuitable because they produce unfavorable line broadening effects. Therefore, factors such as a low total moment and short electron spin relaxation times are equally important considerations. In view of all of these considerations, Eu^{3+}, Yb^{3+} and Ce^{3+} have also become suitable choices (Bentrop *et al*. 1997; Bertini *et al*. personal communication).

Another important consideration is the number of metal binding sites in a macromolecule. Magnetic susceptibility anisotropies are tensorially additive, and depending on the relative orientation of the resulting magnetic susceptibility tensors, constructive or destructive addition may result. Note that in the case of just two sites, it is more likely that the anisotropies will at least partially enhance one another, but with larger numbers of sites cancellation can occur. Many molecules may also have a significant diamagnetic contribution

https://doi.org/10.1017/S0033583500003656 Published online by Cambridge University Press

to the overall magnetic susceptibility tensor. Again, depending on the relative orientation of the paramagnetic and diamagnetic tensors, different levels of net anisotropy can result.

The first example of assisted alignment using non-native paramagnetic centers involved binding of europium ions to two binding sites in a DNA molecule known to form a quadruplex structure in the presence of potassium (Beger *et al.* 1998). Very large $^1D_{CH}$ couplings (-35 to ~ 45 Hz) were measured in this complex at a field strength of 750 MHz. In this striking example, measured residual dipolar couplings were almost one order of magnitude larger than what was observed for the DNA molecule in the absence of the europium ions, or that which was observed for some of the other paramagnetic systems we have discussed thus far.

A broad class of applications involves replacement of native metals in metalloproteins with paramagnetic ions of similar ionic radii. One class of proteins for which this approach has been successfully applied is calcium binding proteins. It has recently been demonstrated that by replacing calcium with Yb^{3+} in the C2A domain of synaptotagmin I, $^1D_{NH}$ couplings in the range of 3 to -2 Hz could be measured (Contreras *et al.* 1999). In order to avoid the unfavorable scenario of destructive addition of magnetic susceptibility tensors from different metal sites, a mutant form of the protein was used to ensure predominant Yb^{3+} binding at one of two binding sites. Isotropic J values could easily be obtained by measuring splittings in the Ca^{2+} form of the protein.

In another application, Ca^{2+} in the N-domain of calmodulin (which has lower affinity to Ca^{2+} than the C-domain) was replaced with Tb^{3+} (Biekofsky *et al.* 1999). This allowed measurement of $^1D_{NH}$ couplings as large as 17 Hz in the N-domain. Moreover, the presence of NMR distinguishable species containing diamagnetic metals allowed simultaneous measurement of isotropic $^1J_{NH}$ values using the same NMR sample. Interestingly, much smaller residual dipolar couplings were measured in the C-domain, attributed by the authors to the presence of conformational flexibility between the two domains.

3.3.2 Advantages of using magnetic alignment

While the domain of applicability remains somewhat limited, there are some unique advantages in using magnetic field alignment. One of these advantages involves selectivity in molecular alignment. For example, one can study the structure of a macromolecular complex, where only one of the participating partners in the complex exhibits a large magnetic susceptibility anisotropy – for example in complexes involving DNA (Tjandra *et al.* 1997). In these cases, measurement of residual dipolar couplings of the less anisotropic partner will result exclusively from its bound state, and these couplings can directly be used to refine the structure of the molecule in the complex. A second advantage is that an independent determination of molecular magnetic susceptibility anisotropy can be used to reduce the number of parameters that must be taken from residual dipolar measurements in the determination of structure or motion (Tolman *et al.* 1997; Banci *et al.* 1998; Volkman *et al.* 1999). For magnetic field alignment of diamagnetic systems, susceptibility tensors can be calculated from the summation of individual group anisotropies when a structural model for the molecule is available (for review see Prestegard *et al.* 1999). For paramagnetic systems, the paramagnetic susceptibility tensor will often dominate the susceptibility, and paramagnetic contribution to the tensor can independently be calculated from the measurement of a sufficiently large number of psuedoconact shifts (Banci *et al.* 1997; Prestegard *et al.* 1999).

Moreover, the measurement of pseudocontact shifts can provide an independent measure of order that is less sensitive to internal motions. This can be very useful for separating contributions to measured residual dipolar couplings which arise from internal motions and from overall molecular alignment (Tolman *et al*. 1997; Prestegard *et al*. 1999).

4. The measurement of residual dipolar couplings

4.1 Introduction

The types of residual dipolar couplings that can be measured in biomolecules has dramatically changed with the introduction of more strongly orienting ordered media. Unlike the early studies on field aligned molecules, where measurements of residual dipolar couplings were primarily limited to directly bonded $^1D_{NH}$ and $^1D_{CH}$ couplings (Tolman *et al*. 1995; Tjandra & Bax, 1997c; Prestegard *et al*. 1999), a variety of single and multiple bond couplings, ^1D, ^2D, ^3D, and longer-range residual dipolar couplings, become amenable to measurement at 0·1% levels of alignment (Tjandra & Bax, 1997a; Tjandra, 1999). This is shown in Fig. 5, where we have predicted the maximum dipolar couplings at 0·1% alignment, between a variety of spins in an idealized polyalanine α-helical segment. Measuring residual dipolar coupling contributions is also more practical at these higher levels of alignment, and can often be done by direct measurement of splittings in frequency domain spectra. There are other advantages that arise when residual dipolar couplings are this large. While extraneous contributions to splittings arising from relaxation interference effects can be significant in magnetically aligned systems (Prestegard *et al*. 1999), these effects do not increase with extent of alignment, and hence become less significant at alignment levels of 0·1% (Tjandra & Bax, 1997a). Consequently, there has been a shift in the development of pulse sequences, from experiments that target the measurement of resonance splittings at sub 0·1 Hz precisions, to experiments that target the measurement of a variety of dipolar couplings in complex molecular systems.

Although a large number of NMR experiments have been developed for the measurements of residual dipolar couplings, we will restrict our attention here to the measurement of $^1D_{NH}$, $^1D_{C^\alpha H^\alpha}$, $^1D_{NC'}$, $^2D_{HNC'}$ and D_{HH}, and for illustration purposes choose experiments that employ different types of NMR methods. Notable experiments that will not be discussed here, are pulse sequences that employ transverse relaxation optimized spectroscopy (TROSY) for improving resolution and for applications to larger systems (Pervushin *et al*. 1997; Yang *et al*. 1999; Permi & Annila, 2000). These are potentially very important experiments, but they have come on the scene only recently, and in most cases can be appended to the experiments we describe.

The NMR methods for measuring coupling constants that we discuss can be divided into two general categories: frequency resolved methods where separation of peak centers is measured in a frequency domain (Montelione & Wagner, 1989), and intensity based experiments, where the coupling is extracted from the resonance intensity rather than from experimental splittings (Billeter *et al*. 1993; Vuister & Bax, 1993; Bax *et al*. 1994). The frequency resolved and intensity based methods are somewhat complementary, as they are often subject to different sources of systematic error. They also differ somewhat in suitability for different types of spin coupling networks: two spin, three spin, and higher.

https://doi.org/10.1017/S0033583500003656 Published online by Cambridge University Press

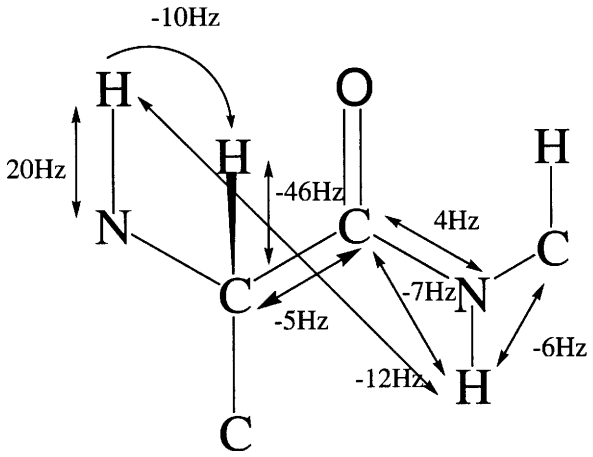

Fig. 5. The predicted maximum value of residual dipolar couplings at ~ 0.1 % levels of alignment for an idealized polyalanine α-helical segment. The alignment is assumed to result in a maximum of 20 Hz $^1D_{NH}$ residual dipolar couplings.

4.2 Frequency based methods

Frequency domain experiments are not only conceptually simple, but are often less prone to systematic errors than resonance intensity based experiments. The simple omission of the normal 180° ^{1}H pulse in the middle of the heteronuclear evolution period of a heteronuclear single quantum coherence (HSQC) experiment provides spectra with J or $J+D$ splittings in the indirect dimension. The measurements of splittings in the indirect dimension is straightforward and often preferred over measurement in the direct dimension because of longer T_2s and fewer cross-correlation distortions of peak positions. However, experiments of this type can suffer from increased complexity as the resulting multiplets produce more peaks than the single peak seen in a decoupled spectrum. Also, they can be time consuming when couplings are measured in the indirect dimension of a two dimensional experiment. To achieve optimum precision, data must be collected for a period of time on the order of the transverse spin relaxation time, T_2, and when peaks are spread over a large frequency range, acquisition of many t_1 points is required. In general, the attainable accuracy and precision of measurement will also highly depend on signal to noise ratio, line shape, number of additional passive couplings, and the method employed for extracting peak positions.

4.2.1 Coupling enhanced pulse schemes

One way to avoid lengthy acquisition is to let the couplings dictate the indirect sweep width (rather than chemical shift dispersion): 2D J-resolved spectroscopy is a long established procedure along these lines, but it does not take advantage of dispersion of resonances due to chemical shift in a second dimension and is seldom applied to large molecules. A modification of 2D J-spectroscopy, in which the indirect evolution period is actually a composite of two evolution periods, incremented accordion style (Bodenhausen & Ernst,

https://doi.org/10.1017/S0033583500003656 Published online by Cambridge University Press

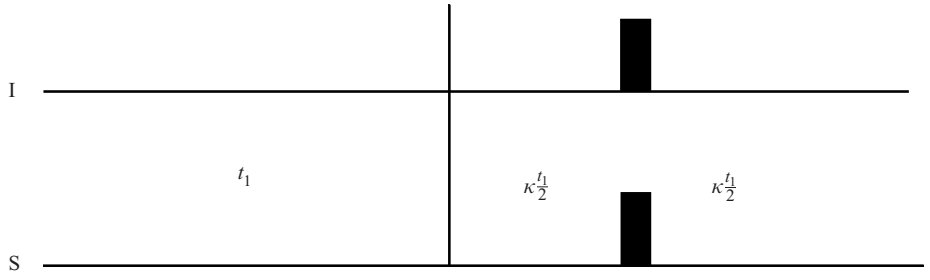

Fig. 6. The 'coupling enhanced' pulse sequence element (Tolman & Prestegard, 1996a). Both pulses are 180° pulses.

1981), provides a useful compromise between spin–spin coupling and chemical shift resolution. We refer to this pulse sequence element as a 'coupling enhanced' element (Tolman & Prestegard, 1996a). This pulse sequence element is shown in Fig. 6. Following magnetization transfer from spin I to spin S using an insensitive nuclei enhanced by polarization transfer (INEPT) element, the evolution period t_1 is divided into two distinct parts. During the first part, both chemical shift and $^1J_{IS}$ coupling evolve exactly as in an (HSQC) experiment, except the 180° pulse normally used to remove I–S couplings is omitted. The t_1 dwell time employed should be short enough to span the S frequencies present and hence is dictated by the S chemical shift dispersion. During the second part, a time of duration κt_1, only pure coupling evolution occurs. Removal of chemical shift and preservation of coupling is accomplished by the inversion of both the I and S spins near the midpoint of this second period. The amount of additional coupling evolution can be varied by modifying the value of the parameter κ. The resulting spectrum is much like that obtained with a simple coupled HSQC experiment, except that the apparent coupling will be larger. Multiple-bond couplings involving the S spin can in certain cases be removed by inserting, at the juncture of the two equal evolution domains, a frequency selective pulse (Emsley & Bodenhausen, 1990) that inverts resonances involved in these additional couplings. An experiment based on this pulse sequence element called a selective coupling enhanced HSQC (SCE-HSQC) has been introduced for measuring $^1J_{NH}$ couplings in proteins (Tolman & Prestegard, 1996a). With a tolerable sacrifice in chemical shift resolution, ^{15}N–^{1}H splittings have been measured using this experiment with an accuracy of 0·2 Hz for a protein the size of 17 kDa. Achieving this precision does, however, require proper methods for extraction of peak positions (Tolman & Prestegard, 1996a).

4.2.2 In phase anti-phase methods (IPAP): $^1D_{NH}$ couplings in proteins

One of the drawbacks of measuring frequency separated doublets in the indirect dimension, particularly for larger proteins, is spectral overcrowding. Many techniques have been introduced for collecting separately each component of the doublet in two different spectra, including spin-state selective excitation (S^3E) experiments (Facke & Berger, 1996; Ross *et al.* 1996; Meissner *et al.* 1997a, 1997b). However, clean separation of doublet components using these techniques is often quite sensitive to the size of the one-bond couplings (Ottiger *et al.*

https://doi.org/10.1017/S0033583500003656 Published online by Cambridge University Press

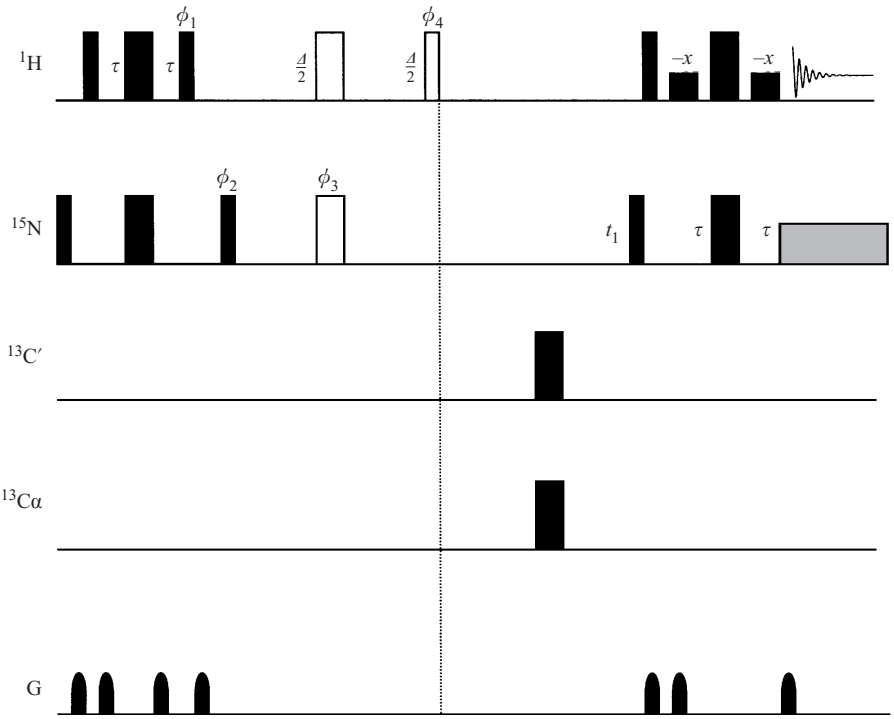

Fig. 7. The IPAP [^{15}N,^{1}H]-HSQC experiment can be used to measure $^1D_{\mathrm{NH}}$ couplings (Ottiger *et al.* 1998a). Narrow and wide pulses correspond to 90° and 180° pulses respectively. The sequence element $\Delta/2-180°(^1\mathrm{H}/^{15}\mathrm{N})-\Delta/2-90°_{\phi 4}$ is only used for generating the anti-phase spectrum (AP) and is omitted for generating the in phase (IP) spectrum.

1998a). While these couplings are largely uniform in isotropic conditions, substantial variations can arise under conditions of alignment due to contributions from dipolar couplings.

A modification to the S^{3}E principle, which is less sensitive to variations in couplings, has been introduced to achieve spin-state separated spectra. This method is based on the collection of two spectra, one where the coupling evolves in phase (IP) and the other where the coupling evolves anti-phase (AP) (Ottiger *et al.* 1998a). Addition and subtraction of these spectra then yields two spectra each with one of the doublet components. In Fig. 7, we show a pulse sequence, IPAP[^{15}N, ^{1}H], designed for the specific measurement of directly bonded ^{15}N–^{1}H couplings in proteins (Ottiger *et al.* 1998a). The pulse sequence can be understood in terms of product operators for two spins I (^{1}H) and S (^{15}N). Generation of the in phase coupling component is simple. Following the INEPT sequence element, one simply allows free evolution of scalar couplings and chemical shift during t_1,

$$2I_z\,\mathrm{S}_y \xrightarrow{t_1} 2\cos(\omega t_1)\cos(\pi J_{\mathrm{NH}}\,t_1)\,\mathrm{I}_z\,\mathrm{S}_y - 2\sin(\omega t_1)\cos(\pi J_{\mathrm{NH}}\,t_1)\,\mathrm{I}_z\,\mathrm{S}_x + \mathrm{IP}, \tag{24}$$

where IP is the in phase term which is not converted back to observable I magnetization. The reverse INEPT transfers magnetization back to protons and yields observable I

https://doi.org/10.1017/S0033583500003656 Published online by Cambridge University Press

magnetization, which is modulated in phase by the couplings $\cos(\pi J_{\mathrm{NH}} t_1)\exp(-\mathrm{i}(\omega t_1))$. In order to obtain the anti-phase component of the coupling, it is necessary to introduce a refocusing period prior to t_1 evolution. This is accomplished using the $\Delta/2-180°-\Delta/2-90°$ sequence element,

$$2\mathrm{I}_z\,\mathrm{S}_y \xrightarrow{\Delta/2-180_x(\mathrm{I,S})-\Delta/2\,90_x(\mathrm{I})} -\sin(\pi J_{\mathrm{NH}}\Delta)\,\mathrm{S}_y, \tag{25}$$

and S_y magnetization evolves into anti-phase magnetization during t_1,

$$\begin{aligned}-\sin(\pi J_{\mathrm{NH}}\Delta)\mathrm{S}_y \xrightarrow{t_1} &-2\cos(\omega t_1)\sin(\pi J_{\mathrm{NH}} t_1)\sin\pi J_{\mathrm{NH}}\Delta)\,\mathrm{I}_z\,\mathrm{S}_x\\ &+2\sin(\omega t_1)\sin(\pi J_{\mathrm{NH}} t_1)\sin(\pi J_{\mathrm{NH}}\Delta)\,\mathrm{I}_z\,\mathrm{S}_y+\mathrm{IP},\end{aligned} \tag{26}$$

where $\mathrm{I}_z\,\mathrm{S}_x$ is now modulated anti-phase by the coupling. The reverse INEPT transfers magnetization back to protons and yields observable I magnetization which is modulated by $\sin(\pi J_{\mathrm{NH}} t_1)\exp(-\mathrm{i}(\omega t_1))$. Addition and subtraction of the two signals followed by Fourier transformation yields individual spectra for each component of the doublet (Ottiger *et al.* 1998a). The IPAP method has also been implemented in a variety of triple resonance NMR experiments (Ottiger *et al.* 1998a).

4.2.3 Exclusive correlated spectroscopy (E-COSY): $^1D_{\mathrm{NH}}$, $^1D_{\mathrm{NC'}}$ and $^2D_{\mathrm{H^NC'}}$ in proteins

Exclusive Correlated Spectroscopy (E-COSY) was originally introduced for the accurate measurement of homonuclear proton couplings that are small compared to line widths (Griesinger *et al.* 1985, 1986; Griesinger & Ernst, 1987), but since the introduction of ^{13}C, ^{15}N isotopic enrichment of proteins, it has also been incorporated into many pulse schemes for measuring heteronuclear couplings. The basic principle of the E-COSY experiment is as follows: a small unresolved coupling J_{IX}, between two spins I and X can be resolved if there is an additional coupling to one of the spins J_{SX}, which is large and well resolved. It must also be possible to transfer magnetization from I to S without perturbing the spin state of the spin X. Usually this is done using I to S coupling, but a more generic transfer is considered here.

In terms of product operators, this experiment appears as follows. Starting with transverse magnetization on the spin S, evolution is described by,

$$\begin{aligned}\mathrm{S}_y \xrightarrow{t_1} &\mathrm{S}_y\cos(\omega_{\mathrm{S}} t_1)\cos(\pi J_{\mathrm{SX}} t_1)-\mathrm{S}_x\sin(\omega_{\mathrm{S}} t_1)\cos(\pi J_{\mathrm{SX}} t_1)\\ &-2\mathrm{S}_x\,\mathrm{X}_z\cos(\omega_{\mathrm{S}} t_1)\sin(\pi J_{\mathrm{SX}} t_1)-2\mathrm{S}_y\,\mathrm{X}_z\sin(\omega_{\mathrm{S}} t_1)\sin(\pi J_{\mathrm{SX}} t_1).\end{aligned} \tag{27}$$

Evolution is followed by a mixing period that selects a quadrature component and transfers magnetization from spin S to spin I without perturbing the X spin,

$$\xrightarrow{\mathrm{mixing}} \mathrm{I}_y\cos(\omega_{\mathrm{S}} t_1)\cos(\pi J_{\mathrm{SX}} t_1)-2\mathrm{I}_y\,\mathrm{X}_z\cos(\omega_{\mathrm{S}} t_1)\sin(\pi J_{\mathrm{SX}} t_1). \tag{28}$$

The I spin evolves during t_2 under the influence of chemical shift and J_{IX} couplings. The two terms that lead to observable operators are,

$$\begin{aligned}\xrightarrow{t_2} &\{\mathrm{I}_y\cos(\omega_{\mathrm{I}} t_2))-\mathrm{I}_x\sin(\omega_{\mathrm{I}} t_2)\}\cos(\pi J_{\mathrm{IX}} t_2)\cos(\omega_{\mathrm{S}} t_1)\cos(\pi J_{\mathrm{SX}} t_1)\,(=\boldsymbol{A})\\ &+\{\mathrm{I}_x\cos(\omega_{\mathrm{I}} t_2)+\mathrm{I}_y\sin(\omega_{\mathrm{I}} t_2)\}\sin(\pi J_{\mathrm{IX}} t_2)\}\sin(\omega_{\mathrm{S}} t_1)\sin(\pi J_{\mathrm{SX}} t_1)\,(=\boldsymbol{B}).\end{aligned} \tag{29}$$

https://doi.org/10.1017/S0033583500003656 Published online by Cambridge University Press

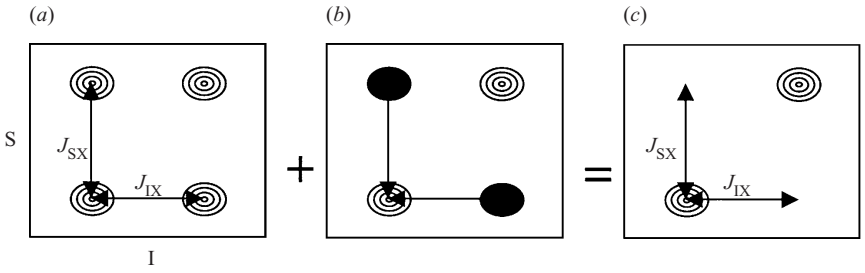

Fig. 8. Schematic depiction of the E-COSY principle. The superposition of a double in phase pattern (*a*) with a double anti-phase pattern (*b*) results in E-COSY pattern (*c*). The black shaded peaks have negative intensity.

The two terms lead to doubly in phase and doubly anti-phase patterns as shown in Fig. 8(*a*) and (*b*). The addition of the two terms (A + B) leads to cancellation of half the multiplet component as shown in Fig. 8(*c*). The requirement that the spin state of the X spin remain unperturbed is easily implemented when the spin X is heteronuclear to both S and I.

While many pulse schemes for measuring *J* couplings utilize this E-COSY principle, we will focus on one experiment that allows the simultaneous measurement of three useful residual dipolar couplings in proteins. In particular, the measurement of $^1D_{C'N}$, as well as $^1D_{NH}$ and $^2D_{H^NC'}$ can be very useful, since all these interaction vectors are fixed in a single peptide plane, the smallest structural element in a protein whose approximate structure can be assumed *a priori*.

In this application the $^2J_{C'H^N}$ ($^2J_{C'H^N} + {}^2D_{C'H^N}$) coupling can be resolved by the $^1J_{C'N}$ coupling (or $^1J_{C'N} + {}^1D_{C'N}$) using an E-COSY scheme. Resolution, and measurement of ($^1J_{NH^N} + {}^1D_{NH^N}$) is achieved using the previously described IPAP[^{1}H–^{15}N]-HSQC pulse sequence (Fig. 7) (Ottiger *et al*. 1998a), with the exception that the 180° pulse on C′ is omitted during t_1, thereby preserving the C′ spin state and allowing $^1J_{NC'}$ coupling evolution (Wang *et al*. 1998b). In analogy to the above description of the E-COSY principle, J_{IX} is $^1J_{NC'}$ and J_{SX} is $^2J_{H^NC'}$. Since the C′ spin state is unperturbed during t_1, an E-COSY pattern such as that shown in Fig. 8 will appear in the resulting pair of IPAP spectra. This experiment has allowed measurement of these three residual dipolar couplings for many amino-acid peptide planes in a 30 kDa deuterated protein (Wang *et al*. 1998*b*).

4.2.4 Extraction of splitting values from the frequency domain

The precision with which a coupling can be measured, particularly when using frequency domain experiments, will depend on the procedure used for extracting coupling values from the spectra. Some of the commonly used software packages include PIPP (Garrett *et al*. 1991) and REGINE (Kleywegt *et al*. 1993). Both these methods employ some form of a parabolic interpolation around a local maximum that allows assimilation of data resident in several adjacent rows or columns of 2D data. Typically, for well resolved peaks with a sufficient signal to noise ratio and well defined line shape, interpolation can improve precision by a factor of 5 or more as compared with the line width of the resonance.

There are some drawbacks in analyzing data converted to the frequency domain with a fast Fourier transform (FFT). Most processed spectra are limited by failure to use all data acquired

https://doi.org/10.1017/S0033583500003656 Published online by Cambridge University Press

(since apodization is needed to remove truncation artifacts from FFT), and the FFT neglects other knowledge about line shapes, amplitude, and phases. There are a number of other well established procedures based on least squares fits to more detailed models that can be used. If we know that our signal is in fact not of fixed amplitude but exponentially decays with rate α, we might consider using an exponentially damped sinusoidal model. In this case, we can replace $\cos(\omega t_i)$ and $\sin(\omega t_i)$ in a typical Fourier transform representation with $\cos(\omega t_i)\exp(-\alpha t_i)$ and $\sin(\omega t_i)\exp(-\alpha t_i)$. The least-squares estimate for ω is then the value of ω which maximizes the real part of the discrete Fourier transform of the 'matched-filter'-apodized FID. This result has been derived within the context of Bayesian parameter estimation (Bretthorst, 1990a, 1990b). If the decay factor, α, is unknown, then both ω and α can be estimated by minimizing the residual sum-of-squares, or equivalently, by maximizing the projection of the model function onto the data. Many methods have been devised for calculating this projection including a method based on generalization of the Clenshaw recurrence relation for finite sums (Andrec & Prestegard, 1998). Alternatively, one could use more direct forms of parameter estimation such as time-domain linear prediction, frequency-domain least squares, or time-domain maximum likelihood (Miller *et al*. 1993; Martin, 1994; Chylla & Markley, 1995).

4.3 Intensity based experiments

Quantitative *J* correlation experiments overcome some of the complexities of frequency domain analysis by encoding coupling in easily quantitated resonance intensity. In these experiments, resolution only needs to be adequate for chemical shift resolution, and intensities can be measured from a single decoupled resonance rather than dealing with signal spread over multiplet components. While extraction of splitting values generally does not require sophisticated data analysis schemes and precisions are very high, there are potential sources of systematic errors (Tolman & Prestegard, 1996b).

4.3.1 *J*-Modulated experiments: the measurement of $^1D_{C^\alpha H^\alpha}$ in proteins

The principle underlying quantitative *J* type experiments is to pass the observed signal through a period in which the intensity is modulated by a known function of the spin–spin coupling (Billeter *et al*. 1993; Vuister & Bax, 1993; Bax *et al*. 1994). Figure 9 shows the pulse sequence for the 2D $^1J_{CH}$-modulated ^{13}C–^1H CT-HSQC experiment, which typifies this class of experiments and which can used for measuring $^1J_{C^\alpha H^\alpha}$ couplings in proteins (Tjandra & Bax, 1997c). An intensity-based experiment is particularly suited for the measurement of $^1J_{C^\alpha H^\alpha}$ couplings in proteins, because C^α nuclei often suffer from poor chemical shift dispersion and broad linewidths. Again the experiment is a modification of the regular HSQC pulse sequence. The 2D $^1J_{CH}$-modulated ^{13}C–^1H CT-HSQC experiment can be understood in terms of simple product operators during the t_1 evolution period. After the first INEPT at the beginning of the pulse sequence, the evolution of antiphase C^α magnetization with respect to a directly bound proton is given by: $^{13}C^\alpha$ chemical shift evolution,

$$2I_z S_y \xrightarrow{T-t_1/2-\Delta-T+\Delta-t_1/2=-t_1} 2I_z S_y \cos(\pi\omega(-t_1)), \tag{30}$$

https://doi.org/10.1017/S0033583500003656 Published online by Cambridge University Press

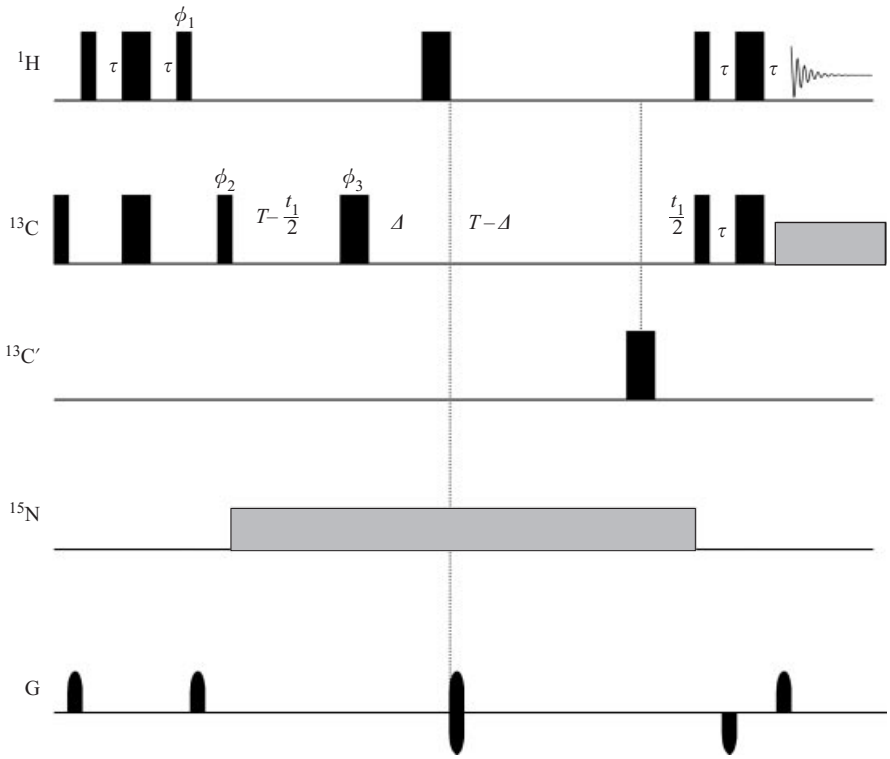

Fig. 9. The 2D $^1J_{\mathrm{CH}}$-modulated ^{13}C–^{1}H CT-HSQC experiment can be used to measured $^1D_{\mathrm{CH}}$ couplings (Tjandra & Bax, 1997c). Narrow and wide pulse correspond to 90° and 180° pulses respectively.

$^1J_{\mathrm{C^\alpha H^\alpha}}$ coupling evolution,

$$2\mathrm{I}_z\,\mathrm{S}_y \xrightarrow{T-t_1/2-\Delta+T-\Delta+t_1/2=2T-2\Delta} 2\mathrm{I}_z\,\mathrm{S}_y\cos\left(2\pi J_{\mathrm{CH}}(T-\Delta)\right), \tag{31}$$

$^1J_{\mathrm{C^\alpha C^\beta}}$ coupling evolution,

$$2\mathrm{I}_z\,\mathrm{S}_y \xrightarrow{T-t_1/2+\Delta+T-\Delta+t_1/2=2T} 2\mathrm{I}_z\,\mathrm{S}_y\cos\left(2\pi J_{\mathrm{CC}}\,2T\right), \tag{32}$$

$^1J_{\mathrm{C\alpha C'}}$ coupling evolution,

$$2\mathrm{I}_z\,\mathrm{S}_y \xrightarrow{T-t_1/2-\Delta-T+\Delta+t_1/2=0} 2\mathrm{I}_z\,\mathrm{S}_y\cos\left(2\pi J_{\mathrm{CC}}\,0\right) = 2\mathrm{I}_z\,\mathrm{S}_y. \tag{33}$$

$^1J_{\mathrm{C^\alpha N}}$ is decoupled throughout t_1. For optimal sensitivity, the constant time delay, $2T$, is set to equal $n\times(1/^1J_{\mathrm{C^\alpha C^\beta}})$, where n is an integer. The intensity of the resulting spectrum will be modulated only by $^1J_{\mathrm{C^\alpha H^\alpha}}$ couplings (neglecting small contributions from long range C–H couplings). By running multiple spectra at different Δ values, the resulting signal intensity modulation can be fit to extract $^1J_{\mathrm{C^\alpha H^\alpha}}$ coupling values (Tjandra & Bax, 1997c). Note that it is important to choose Δ values near a zero crossing, where the resonance intensity will be most sensitive to the $^1J_{\mathrm{C^\alpha H^\alpha}}$ coupling value (Tjandra & Bax, 1997c). For a 17 kDa protein myoglobin, $^1J_{\mathrm{C^\alpha H^\alpha}}$ couplings could be measured with an accuracy of 0·5 Hz when using nine

https://doi.org/10.1017/S0033583500003656 Published online by Cambridge University Press

time intervals (Δ). This experiment has also been modified to allow measurement of couplings in methyl and methylene sites in macromolecules (Ottiger *et al*. 1998b). Other 2D (Hitchens *et al*. 1999) and 3D experiments (Yang *et al*. 1998) have also been devised for measuring $^1J_{C^\alpha H^\alpha}$ couplings in protein systems.

4.3.2 Phase modulated methods

A variation of the above intensity modulation experiment is phase modulation. Like the above experiment, phase modulation depends on the efficiency of transfer of magnetization from one member of a coupled set to another in a typical HSQC experiment. Maximum efficiency is normally accomplished by matching a fixed coupling evolution time, T, to $1/(2(J+D))$. In the normal experiment, part of the signal is lost when the time is not well matched. These intensity decreases could be used to evaluate the degree of mismatch, and hence the value of $(J+D)$. However, the signal normally lost can also be recovered and used to calculate a phase error due to over or under precession during T. This phase error is a function of $(J+D)$ and can be used to evaluate the coupling (see Tolman & Prestegard, 1996b, for the pulse sequence). This experiment is similar in some respects to experiments such as the HNHA in which the referencing is accomplished by observation of a pair of resonances which are cosine and sine-modulated, respectively, by the coupling (Vuister & Bax, 1993). Measurements of the intensities (or peak volume, V_i) of the cosine and sine-modulated components can be related to the angular deviation of coupling evolution, $\Delta(J+D)\,T$ as follows:

$$\Delta(J+D) = \frac{\arctan(V_{\sin}/V_{\cos})}{\pi T}. \tag{34}$$

An experiment, which employs phase modulation, called a phase encoded-HSQC experiment, has been developed for the measurement of $^1J_{NH}$ couplings (Tolman & Prestegard, 1996b). Using this experiment, it is very easy to obtain a precision of 0·2 Hz on a 17 kDa protein, when sources of systematic errors are well accounted for (Tolman & Prestegard, 1996b).

4.3.3 Constant time COSY – the measurement of D_{HH} couplings

As shown in Fig. 5, many long-range D_{HH} couplings can also be observed in proteins, owing to the large magnetogyric ratio of protons. While determining the sign of residual dipolar contributions can be challenging in cases where spins are not scalar coupled (J), even the relative magnitude of these couplings can be indicative of secondary structural types, such as an α-helical geometry, and these couplings can be measured without the need for isotopic enrichment. The primary difficulty in measuring these couplings accurately, is the presence of multiple H–H couplings. In the isotropic solution state, these couplings can often be neglected, and experiments such as the HNHA experiment which measures $^3J_{H^N H^\alpha}$ have been designed in the past for the purpose of obtaining dihedral angle constraints (Vuister & Bax, 1993). However, under conditions of molecular alignment, where a dipolar contribution also exists, multiple H–H couplings can become significantly large, and hence need to be accounted for to allow accurate measurement.

Recently, a simple Constant Time Correlated Spectroscopy (CT-COSY) experiment has been introduced to overcome these 'passive coupling' effects (Tian *et al*. 1999). The very

https://doi.org/10.1017/S0033583500003656 Published online by Cambridge University Press

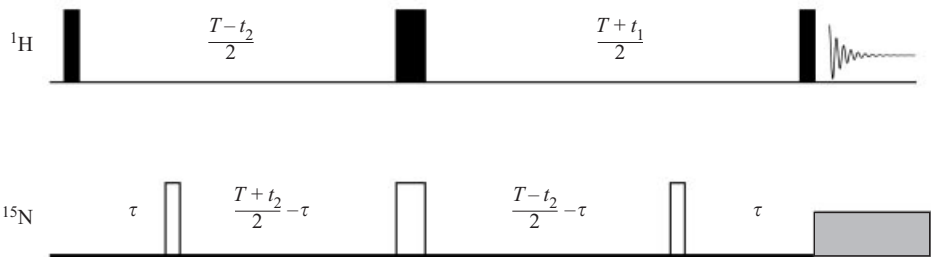

Fig. 10. The CT-COSY experiment can be used to measure D_{HH} couplings (Tian *et al.* 1999). Narrow and wide pulses correspond to 90° and 180° pulses respectively.

simple pulse sequence is shown in Fig. 10. Ignoring the nitrogen channel needed for implementing a 3D, ^{15}N-edited, variation of the experiment for labeled proteins, the CT-COSY pulse sequence element is identical to the traditional COSY experiment, except that a 180° pulse is inserted in between the two 90° pulses where it is moved incrementally from the mid point to one extreme of the constant time period ($2T$). This pulse scheme has previously been proposed for improving sensitivity (Girvin, 1994). However, another property of this pulse sequence proves advantageous in measuring couplings. In the absence of significant differential relaxation, cross-peak intensity for a simple pair of spins experiencing weak scalar coupling and weak dipolar coupling is proportional to $\sin(\pi(J_{12}+D_{12})\Delta)$ while the auto peak intensity is modulated by $\cos(\pi(J_{12}+D_{12})\Delta)$. Hence $J+D$ can readily be obtained from the ratios of auto to cross peak intensities,

$$J+D = \arctan(I_{\text{cross}}/I_{\text{auto}})/\pi\Delta. \tag{35}$$

The presence of additional passive couplings will equally modulate the intensities of both the cross and auto peak by $\cos(\pi(J_{12}+D_{12})\Delta)$, and hence their effects will be largely removed from the calculated ratio. This allows direct measurement of the single active coupling, giving rise to a COSY cross peak, even when many passive couplings are present. There is a problem, however, with the experiment in that intensities must be taken from anti-phase cross peaks. If components are well resolved, this is less of an issue, -but then direct measurement from the frequency domain would also be possible. One solution involves acquiring spectra at multiple Δ delays and plotting the observed amplitude ratio measured at any frequency point as a function of the delay Δ, which is always proportional to $(A_{\text{cross}}/A_{\text{auto}}) = \tan(\pi(J+D)\Delta)$, and $(J+D)$ can be extracted. There are also other experiments that have emerged as means of measuring ^{1}H–^{1}H couplings (Willker & Leibfritz, 1992; Carlomagno *et al.* 1998; Ponstingl, 1998; Cai *et al.* 1999; Heikkinen *et al.* 1999; Pellecchia *et al.* 2000). Some of these are useful for determining dipolar coupling signs (Peti & Griesinger, 2000).

4.3.4 Systematic errors in intensity based experiments

Particularly for intensity based experiments, systematic errors must be carefully considered. Possible contributing errors include hardware timing errors, the effects of gradients and RF-fields applied during critical intensity-coding periods, and the effects of finite pulse widths. It is also important to consider possible effects arising from differential relaxation of $\cos(\pi JT)$ and $\sin(\pi JT)$ components and/or the presence of passive couplings during the intensity-

https://doi.org/10.1017/S0033583500003656 Published online by Cambridge University Press

coding period. The reader is referred to the original works for a treatment of these effects on the pulse schemes reviewed in this section.

5. Interpretation of residual dipolar coupling data

As we have discussed, in just a few years the measurement of large numbers of residual dipolar couplings in multiple order inducing media has become routine. Considering the unparalleled sensitivity of these measurements to small angular displacements, plus the inherently non-local nature of constraints derived, it is not difficult to appreciate that a powerful new tool is now available for the study of biomolecules in solution (Prestegard, 1998). The effective utilization of this huge reservoir of data, either alone or in combination with other types of data, offers some significant benefits beyond just improvements in the precision of structural determination. In principle, independent structural determinations using only orientational constraints could be used for the cross-validation of more traditional NOE-based structures. Of greater significance is the promise of moving beyond the limiting assumption of a single rigid structural model, that has until now been necessary in NMR-based structural studies. These promises have not yet been fully realized, but a review of protocols currently in use, and a treatment of the recent developments that move towards the more effective interpretation of residual dipolar coupling data will illustrate the potential.

5.1 Structure determination protocols utilizing orientational constraints

Thus far, two principal routes have been taken for the utilization of residual dipolar data in structure determination: incorporation of constraints on individual bond orientations as penalty functions within a simulated annealing protocol, and alignment of molecular fragments based on superposition of principal order tensors determined for individual fragments. Although both of these protocols have previously been reviewed in the context of macromolecule structure determination under direct magnetic field alignment (Prestegard *et al*. 1999), we discuss each briefly here.

5.1.1 The simulated annealing approach

The simulated annealing approach has been the one predominantly employed thus far. Residual dipolar couplings are incorporated into the structure calculation by means of a penalty function (Tjandra *et al*. 1997; Nilges *et al*. 1988). This penalty function (equation (36)) is generated by summing, for each measured residual dipolar contribution, the weighted (W) square of the difference between the experimental splitting and the calculated splitting for a trial molecular structure,

$$E_{\mathrm{DD}} = W\sum_i (D_{i,\mathrm{calc}} - D_{i,\mathrm{obs}})^2. \tag{36}$$

This penalty function (or pseudo-energy) is added to normal molecular and NOE distance constraint energies, and a search for a minimum energy structure is conducted using a simulated annealing protocol (Bewley *et al*. 1998; Clore *et al*. 1999; Wang *et al*. 1999). This procedure parallels the one that has been used for years in the determination of structure from

https://doi.org/10.1017/S0033583500003656 Published online by Cambridge University Press

NOE data where observed and calculated interproton distances enter the penalty function. However, there are few additional considerations required in the case of dipolar couplings.

Unlike the reference point in the NOE penalty function, where a distance between atoms can be calculated directly from atomic coordinates (Wüthrich, 1986; Clore & Gronenborn, 1998), the calculation of expected dipolar couplings for a given candidate structure ($D_{i,\mathrm{calc}}$) requires more supplemental information. This can be appreciated by re-considering the equation for residual dipolar couplings derived in the theory section (equation (21)). Calculation of expected values for the dipolar couplings requires knowledge of the two order parameters (S_{zz} and $\eta = (S_{xx} - S_{yy})/S_{zz}$). These parameters are not generally available at the outset of structure determination. In cases where a large number of residual dipolar couplings can be measured, a simple technique for estimating order parameters *a priori* has been introduced (Clore *et al*. 1998b). The success of this technique relies on a sufficiently well-dispersed distribution of residual dipolar coupling measurements (Clore *et al*. 1998a). One further complication arises due to the fact that all of the individual vector orientations are referenced relative to a common molecule fixed frame, which must be allowed to float during the course of simulated annealing (Clore *et al*. 1998a).

5.1.2 Order matrix analysis of dipolar couplings

The order matrix approach begins by dividing a large molecule into a set of small rigid molecular fragments. Under conditions of partial molecular alignment, all fragments in a molecule will experience a common ordering frame, provided that the fragments are part of a properly assembled rigid molecular structure (Losonczi & Prestegard, 1998b; Prestegard *et al*. 1999). Order tensor parameters can be experimentally determined for each fragment, as long as the geometry of the molecular fragment is known relative to an arbitrary frame, and five or more independent residual dipolar couplings are measured (Saupe, 1968). The definition of what constitutes a fragment can vary widely. It can be, for example, an entire protein domain of a multidomain protein assembly, where domain structure may be known from X-ray data, or it can be as small as an approximately rigid pyranose ring in an oligosaccharide, or even a peptide plane if chemical shift anisotropy data can be combined with dipolar data to get a sufficient number of orientational constraints.

A singular value decomposition approach has recently been implemented for efficiently solving for order tensor elements from the linear equations that relate dipolar couplings to order tensor elements (see equation (7) Section 2) (Losonczi *et al*. 1999). Diagonalization of the order matrix formed from these elements yields the principal order parameters (S_{zz}, η) and a transformation matrix. This matrix describes the orientation of the frame of principal order relative to the chosen arbitrary frame of the rigid fragment. For a set of molecular fragments defined in individual arbitrary frames, a complete structure can be assembled by transforming fragment coordinates in the arbitrary frame into the experimentally determined principal order tensor frame, fragment by fragment.

5.1.3 A discussion of the two approaches

A significant advantage of the simulated annealing approach is that it is easy to add residual dipolar pseudoenergy terms to a molecular dynamics force field along with other pseudoenergy terms for NOE and scalar coupling constraints. As the technique is already

mature, and widely used with NOE and scalar coupling data, the determination of detailed and complete structures utilizing all available structural information becomes possible. However, there are some difficulties specifically associated with incorporation of orientational constraints. As mentioned above, simulated annealing requires the prior specification of order tensor parameters. This is particularly difficult for small molecules, but may even be difficult for some large biomolecules, because interaction vectors are prone to be parallel in secondary structural elements (for example, ^{15}N–^{1}H vectors in α-helical and β-sheet structural elements). A more serious limitation arises due to the multiple minima of the penalty function for orientational constraints, and the requirement that the common reference frame be allowed to float. Thus, the long range ordering information potentially contained in the dipolar pseudoenergy term will remain ineffective until a reasonably good structural candidate is obtained. This usually means that the dipolar data is used predominantly in refinement stages, starting with a crude NOE structure, or in combination with large amounts of NOE data. Furthermore, simulated annealing is not particularly amenable to studies that depart from the assumption of a single rigid model for the molecule.

The strength of an order matrix approach is that it allows, simultaneously, a direct solution for fragment orientation and the operative order parameters. The process of solving for fragment orientation is very efficient, allowing repeated solutions from error distributions about measured dipolar couplings to generate a picture of structural precision. The approach can be applied with a relatively small number of residual dipolar couplings, as few as five per molecular fragment, if these give independent information. Moreover, the order tensor approach is naturally suited to problems where a rigid structural model is unacceptable. However, there are also limitations to the order matrix approach. It does require that the fragment structure be known beforehand and that sufficient measurements be available for each and every fragment. It has yet to be demonstrated that this approach can be used to determine, *a priori*, the complete structure of a large biomolecule from a set of data and basic local geometrical constraints. Indeed, applications of the order matrix approach have thus far been confined to either small molecules, or backbone representations of structural elements such as protein domains and secondary structural elements. Furthermore, it is not yet clear how to best combine this approach with other types of NMR data. Thus, it remains that the two approaches have quite different areas of applicability. The suitability of either approach will depend on the system under study, the number of residual dipolar couplings measured, and the amount of structural information available beforehand.

5.2 Reducing orientational degeneracy

One of the inherent limitations that arises in the analysis of dipolar data, regardless of the protocol used, stems from the fact that dipolar coupling measurements do not have a one-to-one correspondence to a pair of polar angles describing the orientation of the interaction vector. A given residual dipolar coupling measurement can only restrict the orientation of the corresponding internuclear vector to two cones (or distorted cones) as shown in Fig. 11. Addition of data corresponding to other vectors rigidly related to the first can reduce the number of possible solutions, but one is never able to reduce solution to a single point.

A consideration of the order matrix approach for molecular fragment assembly can illuminate the origin of this orientational degeneracy. In this case, the degeneracy arises because the relationship between individual vectors and order tensor principle axes depend

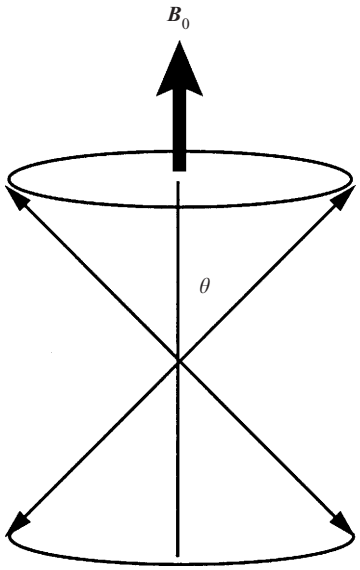

Fig. 11. In the absence of motional averaging, a single residual dipolar coupling measurement restricts the orientation of an internuclear vector to two cones of orientations subtended by the angle θ, relative to the magnetic field.

on $\cos^2\alpha_i$, and are, thus, insensitive to inversion of any of the principal axes of the order tensor. If we insist on maintaining a proper representation of chirality, axes must be inverted in pairs. Hence, two molecular fragments can be assembled relative to one another, but only with a four-fold degeneracy; 'n' molecular fragments can be assembled only with a 4^{n-1}-fold degeneracy (Fig. 12(*a*)). Such degeneracy clearly would limit our ability to define protein structures if only dipolar data were used. In many circumstances, NOE data and/or bonding constraints might be used to overcome this limitation. However, as we discuss below, the most reliable method for reducing this degeneracy is by employing at least a second aligning medium. There are different implications depending upon whether a simulated annealing or an order tensor based approach is used.

5.2.1 Multiple alignment media in the simulated annealing approach

Bax and co-workers first noted that measurement of two independent sets of residual dipolar couplings could restrict the orientation of any one vector to the intersection of two non-coincident cones of solution (Ramirez & Bax, 1998); usually four points. Note that a simple change in the extent of alignment does not change the shape or orientation of the cone, and hence, results in intersection of the entire surface. Once appropriate data are obtained, however, it is straightforward to include a second set of residual dipolar couplings in the simulated annealing procedure. One simply includes another penalty function and set of order tensor parameters for the new set of residual dipolar coupling measurements (Clore *et al.* 1999). Using this approach, Clore *et al.* observed an increase in the precision of structure determination of the B1 domain of streptococcal protein G by 20–30% (Clore *et al.* 1999). Moreover, inclusion of two independent sets of residual dipolar couplings reduced the number of NOE constraints needed to obtain reasonable structures.

https://doi.org/10.1017/S0033583500003656 Published online by Cambridge University Press

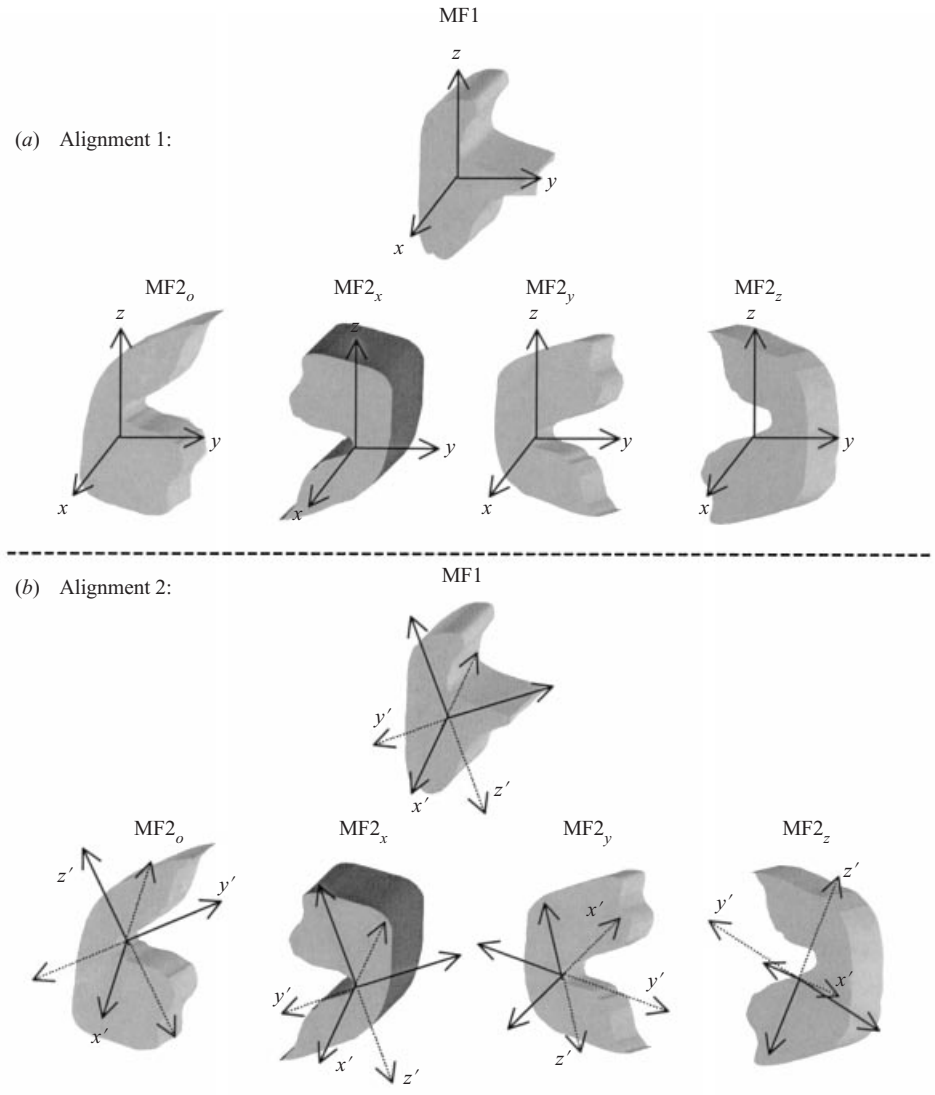

Fig. 12. Resolving orientational degeneracy using two non-coincident order tensors. (*a*) The four possible ways to assemble two molecular fragments using a single order tensor frame from alignment medium 1. Note that while the molecular orientations $MF2_o$, $MF2_x$, $MF2_y$ and $MF2_z$ will always be distinguishable for non-symmetrical molecules, the designation 'o', 'x', 'y' and 'z' is arbitrary. (*b*) The orientation of the order tensor frame (x',y',z') using alignment medium 2 from the point of view of the molecular orientations shown in Fig. 12(*a*). Only one of the four possible orientations ($MF2_x$ shaded in dark gray) has a coincident order tensor frame with MF1.

5.2.2 Multiple alignment media in the order matrix approach

The four-fold orientational degeneracy encountered using the order matrix approach and a single alignment medium can be completely removed by including just a second set of residual dipolar couplings. The approach used in combining data is illustrated in Fig. 12(*b*) (Al-Hashimi *et al.* 2000b). Briefly, measurement of five or more independent residual dipolar

https://doi.org/10.1017/S0033583500003656 Published online by Cambridge University Press

couplings in each molecular fragment, MF1 and MF2, allows determination of order tensor elements and a principal alignment frame for each. Structure determination then proceeds by aligning the resulting principal order frames. For two molecular fragments, MF1 and MF2, this gives rise to four unique relative orientations that are consistent with residual dipolar coupling measurements (Fig. 12(*a*)). If a new set of residual dipolar coupling data is recorded using a second aligning medium, that produces a new non-coincident order tensor orientation. One can analogously generate a new set of four possible orientations of MF2 relative to MF1. Fragment MF1 can now be oriented identically for the two sets (Fig. 12(*b*)), and the relative orientations for MF2 in the two media compared. One finds that fragment orientation is identical in only one case. This corresponds to the correct orientation of MF1 relative to MF2 (dark grey fragments).

This approach has been demonstrated for two fragments in the protein rubredoxin (Al-Hashimi *et al*. 2000b). The determined orientation of two molecular fragments using this procedure proved to be in excellent agreement with the available crystal structure. Note that the inherent resolution in discriminating between the various orientational solutions using this approach will in general depend on both the level of non-coincidence between the two order tensors and the precision with which these orientations can be determined.

5.3 Simplifying effects arising due to molecular symmetry

As was recognized as early as the 1960s in the field of liquid crystal NMR, molecular symmetry can simplify analysis of residual dipolar data and reduce the number of independent parameters in an order tensor analysis (Saupe, 1968). These simplifications can be applied not only to symmetrical molecules, but, notably, to homomultimeric complexes as well. Structural studies of homomultimeric systems have traditionally been difficult by NMR because of an inability to distinguish intersubunit from intrasubunit NOEs (O'Donoghue & Nilges, 1999).

In general, homomultimeric complexes have point group symmetry (O'Donoghue & Nilges, 1999). A point group 'n', where n is an integer, indicates that n monomeric units are related by n-fold rotation; multiple rotational symmetry relations are denoted by appending additional integers to characterize these relations. For example, 22 indicates a tetramer formed by first generating a dimer through a 2-fold rotation of a monomer, and second, generating a tetramer through another 2-fold rotation of the resulting dimer about an axis perpendicular to the first. For symmetric macromolecular aggregates, only the following point groups are possible: n, $n2$, 23, 432, 532, where n is a positive integer (Weyl, 1952).

These point group symmetries have specific implications for an order tensor analysis. For n ($n \geqslant 3$), $n2$ ($n \geqslant 3$), 432 and 532 point group symmetries, the order tensor will be axially symmetric ($\eta = 0$), and the direction of principal order (S_{zz}) will point along the principal axis of symmetry (Saupe, 1968; Al-Hashimi *et al*. 2000a). In the case of $n = 22$ point group symmetry, order tensor axes will point along the orthogonal 2-fold symmetry axes. One of the principal axes will point along the 2-fold symmetry axis in cases of $n = 2$ point symmetry. These relationships can be useful as principal axis directions can be determined independently of any measured data, reducing the number of variables in the order tensor analysis. These sorts of simplications were advantageous for a determination of the ligand-bound geometry of a carbohydrate molecule in fast exchange with a homomultimeric protein with $n = 3$ point group symmetry (Bolon *et al*. 1999). Analogously, symmetry considerations can render the

https://doi.org/10.1017/S0033583500003656 Published online by Cambridge University Press

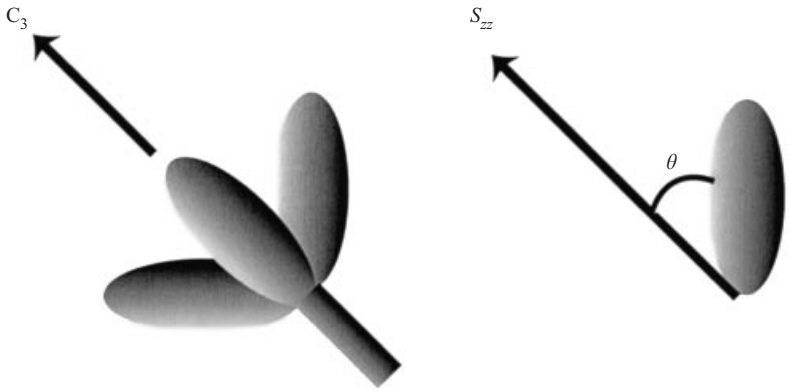

Fig. 13. The use of C_3 molecular symmetry in structure determination of homomultimers using residual dipolar couplings and an order matrix approach. The order tensor is dictated by molecular symmetry, with the principal axis (S_{zz}) pointing along the symmetry axis (note axial symmetry implies $\eta = 0$). Determination of S_{zz} orientation allows specification of the position of the symmetry axis relative to the individual molecular fragment. This allows assembly of the homomultimeric complex.

problem of orienting one domain of a multimer relative to an axis of symmetry almost trivial, as illustrated in Fig. 13 (Al-Hashimi *et al*. 2000a).

5.4 Database approaches for determining protein structure

Difficulties in producing *ab initio* structures using dipolar data alone have prompted the development of new protocols. Recently it has been proposed that the PDB database itself can be used to supply candidate structures, which are then screened using a set of measured dipolar couplings. As demonstrated by Annila *et al*. (1999), homologous protein structures give rise to similar patterns of residual dipolar couplings. To implement screening, the principal order parameters (S_{zz}, η) are first computed from the distribution of measured residual dipolar couplings (as described in Section 5.1.1). The orientation of the order tensor is then allowed to float during a least squares fitting procedure that attempts to reproduce measurements using the rotated coordinates of the candidate structure in the database. The authors demonstrated that homologous proteins could be identified by the fact that only homologous structures would lead to an rmsd between measured and predicted couplings which approached experimental error.

In an extension of this approach, Bax and co-workers developed a procedure called 'molecular fragment replacement' (Delaglio *et al*. 2000). In this case the protein is divided into segments (seven amino-acids proved optimal), and a similar search against the protein database is conducted to find a best match between measured residual dipolar couplings and values predicted for a given structural fragment. Chemical shift measurements were included as well in the search, in order to help reduce the degeneracy of orientational solutions. Using a method analogous to the order tensor–singular value decomposition analysis, to improve efficiency a very large set of fragment geometry representations in the PDB were screened for consistency with dipolar coupling data. When multiple acceptable fragments are found to have ϕ and ψ combinations that cluster in Ramachandran plots, the fragment geometry is adopted. Since fragments are chosen in all possible combinations and overlap extensively, a

https://doi.org/10.1017/S0033583500003656 Published online by Cambridge University Press

complete structure for a protein can be generated. Using this procedure, Bax and co-workers were able to determine the structure of ubiquitin with an rmsd of 1 Å relative to the X-ray structure. These and other studies indicate that there will be new avenues for determining protein structures using residual dipolar couplings in the near future (Meiler *et al*. 2000).

6. Applications to the characterization of molecular systems

Residual dipolar couplings are now being used to address a number of different problems in structural biology. These range from high resolution structural applications to proteins, to the determination of inter domain orientation in multi domain or multi subunit systems, to characterization of structure and dynamics of non-protein systems such as oligosaccharides, or ligands bound to receptors. A variety of different dipolar interactions have been employed, using different techniques described in Section 5. In what follows, we attempt to give just a sampling of the types of applications that are emerging with specific discussion restricted to aspects of direct relevance to the use of dipolar coupling derived constraints. We have focused primarily on proteins and oligosaccharides because of our own interests. Notable applications that we do not discuss include those involving structure determination of isolated oligonucleotides (we do treat an RNA-protein complex later in this section). This is an important area, since the low proton density and the extended nature of these molecular systems has rendered their structure determination by traditional NMR techniques very challenging. Reports of measuring residual dipolar couplings in these systems exist, and structural work is in progress (Beger *et al*. 1998; Clore *et al*. 1998c; Hansen *et al*. 1998; Hoogstraten & Pardi, 1998). We apologize in advance for omitting a detailed discussion of these studies.

6.1 Protein structure refinement

A number of protein structures have now been determined using a combination of residual dipolar coupling data and traditional NOE data. These applications have primarily used the simulated annealing protocol, and provide a useful basis for evaluating the impact of including residual dipolar data on structure determination by NMR. In Table 1, a comparison of resulting structural quality is made, before and after adding orientational constraints. It is clear that incorporation of residual dipolar constraints can significantly improve the precision of structures determined by NMR. This is partly due to a simple increase in structural constraints, and partly due to the fact that residual dipolar couplings can be measured at very high precision. Moreover, because of the orientational nature of these constraints, the measurements are highly complementary to NOE-derived distance constraints, and hence provide a largely independent set of structural constraints. The number of residual dipolar data used in these applications can vary, but they can often be as few as one N–H angular constraint per residue. On average, precision (measured as rmsd of backbone atoms) has increased by 0·5 Å, to a level under 1 Å. It is interesting to note that not only precision, but also accuracy improves. Accuracy has been evaluated by comparison to high resolution X-ray structures when they are available. There will of course be exceptions to this agreement, particularly in less structured regions at the surfaces of proteins. Note that Clore *et al*. have also introduced an R-dipolar factor for assessing the quality of structures determined using

Table 1. *Impact of adding residual dipolar coupling measurements on structures determined using simulated annealing*

	No Dipolar Data		With Dipolar Data	
Structure	Precision (Å)	Accuracy (Å)	Precision (Å)	Accuracy (Å)
GB1	2·88	4·33	1·37	1·12
BAF	1·31	1·37	1·23	0·91
CVN	1·67	1·53	1·23	1·10
FK506	0·67	1·12	0·29	0·74
GATA-1	0·76	NA	0·68	NA
KH	0·39	NA	0·16	NA
SAΔ41	0·71	NA	0·65	NA

Precision is the backbone rmsd for ensembles of structures calculated using simulated annealing. For calculation of accuracy, see original manuscripts. GB1 = B1 domain of streptococcal protein G (Clore *et al*. 1999), BAF = the monomer of the barrier-to-autointegration factor (Clore *et al*. 1999), CNV = cyanovirin-N (Clore *et al*. 1999), FK506 is in complex with FKBP (Olejniczak *et al*. 1999), GATA-1 = transcription factor in complex with a 16 base pair oligodeoxyribonucleaotide (Tjandra *et al*. 1997), KH = Gly26 → Arg mutant of the C-terminal K-homology (KH) domain of hnRNP K (Baber *et al*. 1999), S4Δ41 = Residues 43–200 of S4 (Markus *et al*. 1999).

dipolar coupling data (Clore & Garrett, 1999). We expect that orientational constraints will be used increasingly in NMR protein structure determination (Cai *et al*. 1998; Skalicky *et al*. 1999).

6.2 Protein domain orientation

Because residual dipolar data can constrain the spatial relationship of even remote parts of molecules, it provides a unique opportunity to explore structural features in higher levels of protein organization. Determining relative domain orientation in multi-domain (or multi-subunit) proteins is an important issue, particularly because the functional properties of many of these systems are predicated on specific domain–domain interactions.

Establishing relative domain orientation using traditional NMR methods can be difficult in cases where domains are too distant from one another to allow measurement of a useful number of inter-domain NOE contacts. There are also problems with ambiguity of NOEs when dealing with homomultimeric proteins, where intra and inter sub-unit interactions between the same pairs of protons become indistinguishable. There has been some progress in the use of spin relaxation measurements to fix domain orientation; however, these applications do require that the protein molecule have a sufficiently anisotropic diffusion profile (Fushman *et al*. 1999; Tjandra *et al*. 1996). While X-ray crystallography has successfully been employed to determine structures of multi-domain proteins, crystal-packing forces can affect relative domain orientation, and lead to departure from the average and physiologically relevant conformation present in solution.

Fischer *et al*. have investigated the utility of residual dipolar couplings in defining relative domain orientation in an engineered two domain fragment (domains B and C; 88 amino-acid residues) of the barely lectin protein (BLBC) (Fischer *et al*. 1999). Each domain binds specific carbohydrate ligands, and the relative orientation of the two domains is particularly important, because simultaneous binding to multiple domains is used as a general mechanism to amplify binding affinity. A low resolution structure of this protein was previously

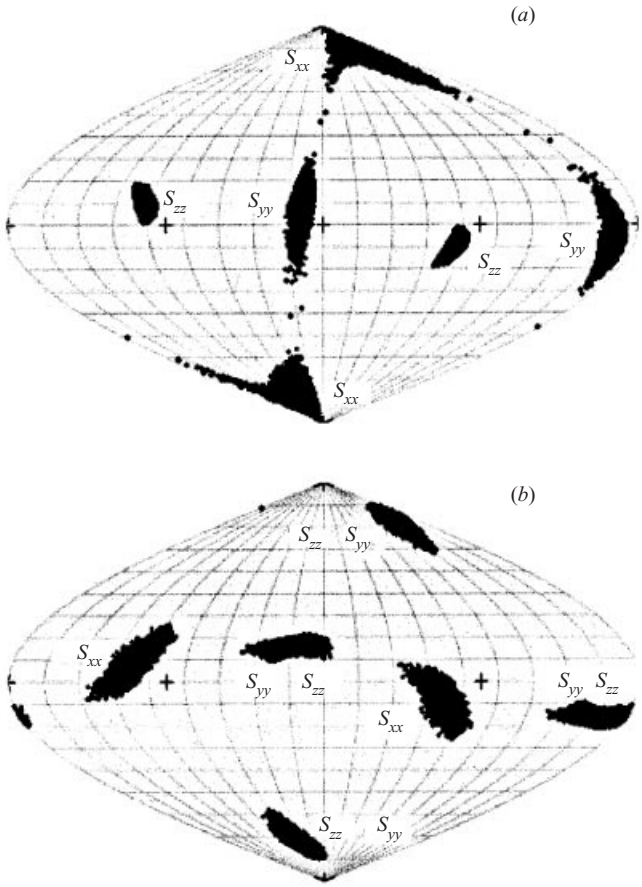

Fig. 14. A Sauson–Flamsteed plot depicting the orientation of the order tensor principal axis system for (*a*) domain B and (*b*) domain C, of the protein BLBC dissolved in a bicelle doped with 5% CTAB. The Sauson–Flamsteed projection maps the surface of a unit sphere into a plane by converting latitude (ϕ) and longitude (λ) to Cartesian coordinates (x,y) via $y = \phi$ and $x = \lambda \cos \phi$. The horizontal lines of latitude run from $-90°$ to 90° in 10° increments, while vertical curved lines of longitude run from $-180°$ to 180° in 20° increments. Any point in this plot represents the orientation of, relative to the chosen arbitrary frame, a determined principal ordering axis. The labeling ambiguity in panel (*b*) is because the asymmetry parameter, η, has a value close to 1.

determined using traditional NOE-based methods, but very few inter-domain NOEs were observed, and the relative positioning of the two domains was poorly defined (Weaver & Prestegard, 1998).

In order to establish the relative orientation of the two domains, $^1D_{\mathrm{NH}}$ couplings were measured with the protein dissolved in two dilute bicelle media, doped with different levels of positively charged cetyltrimethylammonium bromide (CTAB), 2·9% and 5% relative to DMPC, respectively. Doping bicelles with CTAB was used here to discourage protein association with the bicelle particles. The number of NOEs used in the determination of the low resolution NMR structure was insufficient to productively pursue a structure determination using a simulated annealing approach. Instead, an order matrix approach was adopted, in which each domain was assumed to have an internal backbone structure superimposable with the structure of the closely homologous protein wheat germ agglutinin

https://doi.org/10.1017/S0033583500003656 Published online by Cambridge University Press

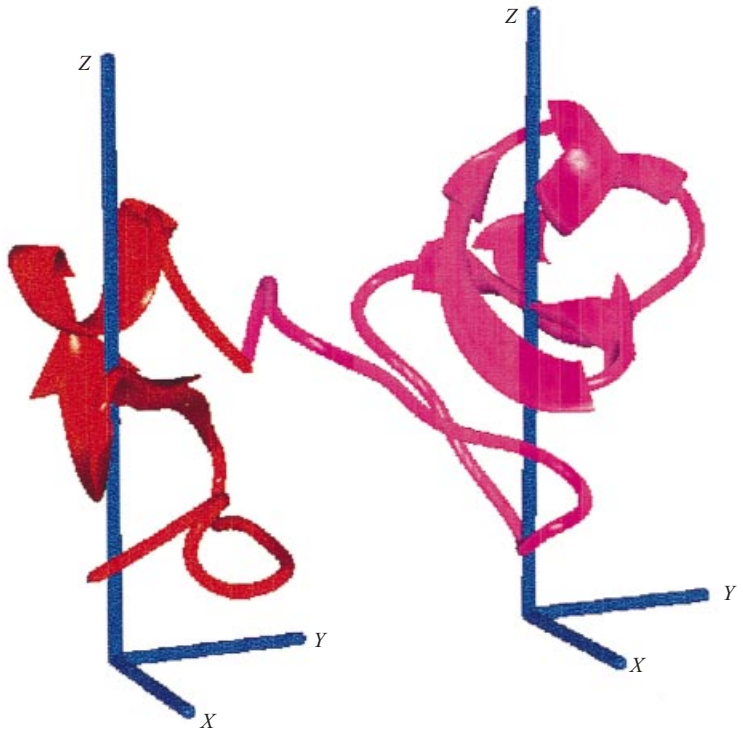

Fig. 15. The relative orientation of domain B and C in BLBC obtained by superimposing the independently determined order tensor frames (shown in Fig. 14).

(WGA), for which an X-ray structure was available. Only dipolar couplings in the well structured core region of BLBC that shares sequence similarity to WGA was used, and order tensor elements were independently determined for two sets of $^1D_{NH}$ couplings measured in the two bicelle preparations respectively. A total of just 13 and 21 $^1D_{NH}$ couplings were used in the order tensor determination for domain B and C respectively.

In Fig. 14, we show calculated solutions for order tensor allowed orientations for each domain using a Sauson–Flamsteed projection (Losonczi & Prestegard, 1998b) (see figure legends for a description of the Sauson–Flamsteed projection). Resulting orientations were well determined, however, reassembly of domains, based on the superposition of domain–fixed order tensor frames for the 5% doped CTAB preparation, resulted in structures that deviated from the WGA X-ray structure. The structure, which is shown in Fig. 15, is consistent with all other previously determined NOE constraints, so, the departure from the X-ray structure are very likely real. However, this is a domain fragment cut from a protein that normally contains four domains in a dimer.

There are other indications of structural instability in the two domain fragment. In Fig. 16, we show a histogram plot of calculated order parameters for individual domains. For the weakly doped bicelle media, the order parameters determined for domain B and C differed by a factor of 3 (Fig. 16), and this difference was attenuated in the bicelle media doped with a larger amount of CTAB. The authors proposed that the large difference in observed order parameters was due to partial association of one of the domains (domain B) with the bicelle particles. Under these circumstances, where one domain is preferentially restrained, the

https://doi.org/10.1017/S0033583500003656 Published online by Cambridge University Press

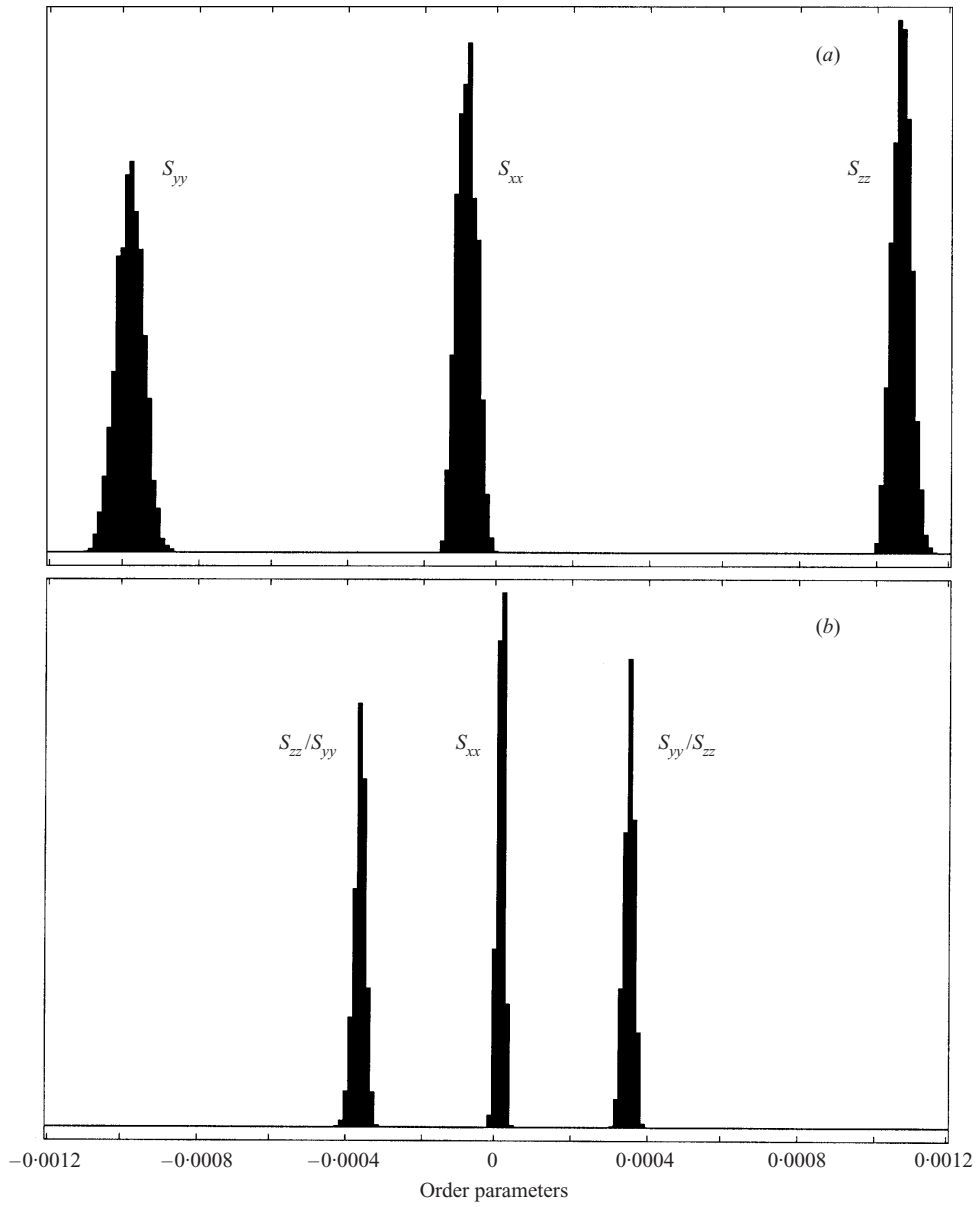

Fig. 16. Histogram plot of calculated order parameters for domains B and C in BLBC, dissolved in a bicelle doped with 2·9 % CTAB, panels (*a*) and (*b*), respectively. Panel (*b*) displays an ambiguity because the asymmetry parameter, η, has a value close to 1.

difference in calculated order can be used to estimate amplitudes of motion; in this particular study, motional amplitude was estimated to be on the order of $\pm 40°$. In addition to highlighting the potential for using residual dipolar couplings to investigate both structure and motion, this study also suggests that caution is necessary in interpreting the average structure of such loosely connected multi-domain systems in terms of a rigid model.

In another study, Kay and co-workers determined the relative orientation of two domains in the matlodextrin binding protein (MBP) using extensive residual dipolar coupling

https://doi.org/10.1017/S0033583500003656 Published online by Cambridge University Press

measurements (Skrynnikov *et al*. 2000). MBP is a 370-residue protein composed of two comparably sized domains connected by two β-strands and a relatively long stretch of α-helix. The ligand binding properties of this protein are intimately connected with the relative orientation of these domains, which can assume both an open and closed conformation. X-ray data indicate that these conformational changes are related by hinge rotations of one domain with respect to the other. These conformational changes are crucial for MBP's role in the signal transduction cascade that regulates both maltodextrin uptake and chemotaxis.

The solution structure of MBP was previously determined using traditional NMR techniques. However, the small number of weak NOEs observed between the two domains again did not allow accurate determination of relative domain orientation. In order to determine the relative orientation of the two domains, a total of 1356 dipolar couplings were measured (^{15}N–^{1}H, ^{15}N–^{13}C′, ^{13}C–^{13}C′, ^{13}C′–HN, ^{13}C–^{1}H) for β-cyclodextrin loaded MBP in phage media. Beginning with four X-ray structures for MBP (two displaying open conformations and two closed conformations), a minimization algorithm was designed to search for the hinge rotation that provides the best agreement between the measured and calculated residual dipolar couplings. The determined solution structure indicates that MBP is more closed that what is observed in the X-ray open structures. These results were also consistent with other results from spin-labeling studies, and analysis of anisotropic rotational tumbling based on ^{15}N relaxation parameters. The authors suggested that the difference between the X-ray structure and the determined solution structure is due to crystal packing forces, which are thought to be extensive in this form of MBP. Other applications in this area include the determination of the relative orientation of two sub-domains in the ribosomal protein S4Δ41 (Markus *et al*. 1999).

6.3 Oligosaccharides

Use of residual dipolar coupling data in the structural analysis of molecules other than proteins has also proven valuable. We illustrate this point by highlighting some applications to oligosaccharides. Structure determination of oligosaccharides has traditionally relied on the measurement of inter-residue NOEs for distance constraints and inter-glycosidic ^{3}J scalar couplings for dihedral constraints. The primary limitations of these techniques are that it is often difficult to measure a large number inter-residue NOEs, and that one must rely on successive short-range constraints to dictate spatial relationships of remotely positioned residues. In addition, both measurement and interpretation of NOE data can be difficult in these smaller, often flexible molecules. NOEs are nearly zero, regardless of distance of separation for molecules with correlation times that approach the reciprocal of the larmor precession frequencies. Moreover, when NOEs are near zero, they can be exceedingly sensitive to variations in effective correlation times due to diffusional anisotropies. When internal motions exist, variations in effective correlation times for any given interaction vector becomes even more of a problem. While rotating frame measurements, and more complete spin relaxation analysis can help, collecting the additional data is often an arduous process. Use of residual dipolar coupling data can provide a more fruitful approach to a structural and dynamic characterization.

While applications to oligosaccharides date back to 1989 (Ram *et al*. 1989), one of the first modern illustrations of the structural utility of residual dipolar couplings for soluble oligosaccharides was reported by Homans and co-workers, in a study of a ^{13}C-enriched

trisaccharide moiety from the ganglioside Gm3 (Gm3–OS, Neu5Acα2–3Galβ1–4Glc) (Kiddle & Homans, 1998). A total of 13 $^1D_{CH}$ couplings were measured in this trisaccharide dissolved in a dilute bicelle solution. The residual dipolar couplings were incorporated into a simulated annealing protocol, and two families of structures were generated that were consistent with the measured dipolar coupling data (they differed in the Galβ1–4Glc glycosidic linkage; $\phi, \psi \sim (15°, -18°)$ and $(62°, +15°)$, respectively). The existence of these conformations had been suggested by a previous study of this trisaccharide and were, as well, populated during a 5 ns molecular dynamics simulation. Soon after this study, Rundlof *et al.* demonstrated that $^1D_{CH}$ couplings measured in a tetrasaccharide found in human milk (moleculelacto-N-neotetraose (LNnT) β-D-Galp-(1-4)-β-D-GlcpNAc-(1-3)-β-D-Galp-(1-4)-D-Glcp) were consistent with a cylindrical model for the carbohydrate molecule, generated using a molecular mechanics calculation (Rundlof *et al.* 1998).

Recently, a more extensive study by Bush and co-workers has appeared, in which the conformation of six oligosaccharides found in human milk, varying in size from four to six residues, was explored (Martin-Pastor & Bush, 2000). This study illustrated some of the difficulties encountered in the analysis of residual dipolar couplings in carbohydrate molecules. The study extensively relied on the measurement of one-bond $^1D_{CH}$ couplings. This can be insufficient, as many C–H bond vectors are parallel in sugar rings (for example all axial protons in the $^4C_1$ chair conformation), and no more than three independent C–H internuclear vector orientations are typically observed. In the absence of other residual dipolar coupling measurements (for example $^2D_{CH}$ and D_{HH}), it is difficult to either estimate order tensor parameters needed for the implementation of a simulated annealing protocol, or treat sugar rings as individual fragments in the direct application of an order matrix approach. Another problem arises due to the presence of internal motions between residues. While rings themselves can often be assumed rigid, motion about the glycosidic bond connecting sugar residues can complicate analysis of residual dipolar couplings in terms of a single static conformation.

Bush and co-workers proceeded by making use of the previously determined conformations of the Lewis epitopes in these oligosaccharides, which include at least three residues. It is suspected that residues constituting the Lewis epitopes are largely rigid. Starting with only the three residues of the Lewis epitope, a set of energy-minimized conformations was derived that was in agreement with previously measured inter-residue NOEs. Since five independent $^1D_{CH}$ couplings could be measured in the Lewis epitope when it is considered as one entity, order tensor parameters could be determined with reasonable certainty. Additional residues were then added to the epitope core, one residue at a time, while the Lewis epitope conformation was held fixed. A grid search and energy minimization was then preformed for the newly formed linkages, and for each conformation, residual dipolar couplings were calculated and compared to measured values. Conformations that best agreed with measured residual dipolar couplings were selected as candidate structures. The authors report that for four of the oligosaccharides studied, the allowed conformations determined using residual dipolar couplings were in agreement with previously measured inter-residue NOEs, and this fact lead the authors to suggest that newly added linkages in these four oligosaccharides were also largely rigid. Similar conclusions, however, could not be reached for the two remaining oligosaccharides studied.

In another study on a trisaccharide molecule, methyl 3,6-di-O-(α-D-mannopyranosyl)-α-D-mannopyranoside (Triman), Tian *et al.* explored the possibility of determining an average

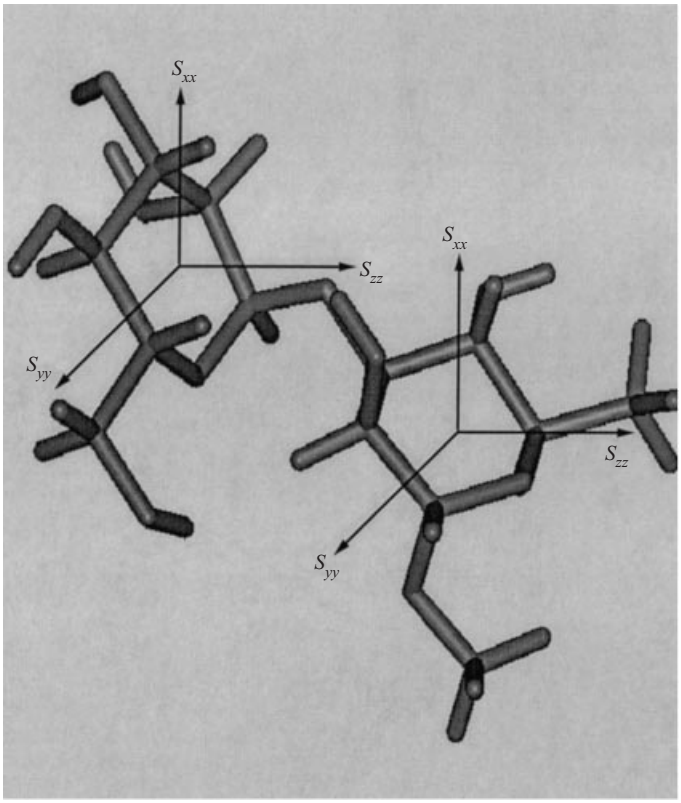

Fig. 17. The structure of ring I and ring III in the trisaccharide Triman (see text), assembled by superimposing determined order tensor frames.

structure for the molecule while also addressing the presence of internal motion (Tian *et al.* personal communication). An order matrix approach was employed with each of the sugar rings treated as rigid fragments of known geometry. $^{1}D_{\mathrm{CH}}$, $^{2}D_{\mathrm{CH}}$ and D_{HH} couplings were measured, resulting in at least six measurements per fragment. Dipolar couplings were also measured using both phage and bicelle media, in order to eliminate the four-fold degeneracy encountered in aligning order tensor frames for the three residues.

An assessment of internal dynamics was made by consideration of the generalized degree of order (GDO) (see Section 2), determined individually for each ring. The GDO parameters for the 1–3 linked ring (I) and the central ring (III) were similar, while the GDO measured in 2–6 linked ring (II) was reduced by 40 %. This pattern was observed in data collected in both media, and suggests that internal mobility between ring I and III is moderate, while there is much larger mobility between ring II and ring III. This picture is consistent with previous studies and expectations based on the extra degree of freedom in the 1–6 glycosidic linkage. The relative orientation of the I and III rings was determined by superimposing determined order tensor frames and the resulting mean structure is depicted in Fig 17.

6.4 Biomolecular complexes

The problems encountered in the structural characterization of biomolecular complexes are similar to those encountered in multiple domain systems. Again, the use of residual dipolar

https://doi.org/10.1017/S0033583500003656 Published online by Cambridge University Press

data can help overcome some of these traditional limitations. The first application of residual dipolar couplings in structure refinement of a heterologous macromolecular complex dates back to the classic study of Tjandra and co-workers on the transcription factor, GATA-1, complexed to a 16 base pair DNA double helix. This system was magnetically aligned due to DNA's large magnetic susceptibility anisotropy (this study has previously been reviewed by Prestegard *et al*. (1999)) (Tjandra *et al*. 1997). The structure of the GATA-1–DNA complex had been solved previously by conventional NMR methods. The addition of $^1D_{NH}$ and $^1D_{CH}$ couplings, measured in the protein, to the simulated annealing protocol shifted many backbone torsion angles into more favorable regions of the Ramachandran map as well as better defining the structure of a loop that displayed few NOE contacts (see Table 1).

More recently, Bayer *et al*. explored the utility of using residual dipolar couplings in the structure determination of a complex between human U1A protein ($\sim$ 100 amino-acid residues) and the polyadenylation regulatory RNA element (Bayer *et al*. 1999). While the structure had been previously determined to excellent precision using over 2500 distance and dihedral angle constraints, the orientation of the RNA double helical regions at the protein–RNA interface were poorly defined. In an attempt to establish these orientations more accurately, 86 $^1D_{NH}$ couplings were measured in the protein and 34 couplings were measured in the RNA (nine imino NH pairs, 16 base CH pairs and nine sugar CH pairs). A dilute bicelle medium was used to achieve partial orientation and the orientational constraints were introduced into the simulated annealing procedure used to determine the structure of the complex. Inclusion of residual dipolar couplings did not significantly affect the precision of structure determination; however, significant changes in the global orientation of the RNA element were observed.

Wright and co-workers have employed residual dipolar couplings to examine more closely discrepencies in relative orientation of two zinc-finger domains, as determined by NMR and X-ray crystallography. In a complex involving the transcription factor IIIA (TFIIIA) bound to the cognate DNA (Tsui *et al*. 2000), there are substantial differences between relative orientation of the first and second amino-terminal zinc-finger in the NMR and X-ray derived structures. A new structure determination was pursued, using a simulated annealing protocol that included a set of measured $^1D_{NH}$ and $^1D_{CH}$ couplings. The resulting structures exhibited notable improvement in overall precision (from 0·63 Å to 0·39 Å), and even more significant improvements in precision of determination of the relative zinc-finger domain orientations (from 1.21 Å to 0·58 Å). The relative orientation of zinc-finger 1 and zinc-finger 2 that agreed best with measured residual dipolar couplings, was determined to lie in between the orientations determined by X-ray crystallography and originally by NMR.

Other examples of application to biomolecular complexes exist and this area is certain to continue to grow. For example, residual dipolar constraints were included in the structure determination of a 40 kDa complex formed between the N-terminal domain of enzyme I (EIN) and the histidine-containing phosphocarrier protein (HPr) (Garrett *et al*. 1999).

6.5 Exchanging systems

A special class of biomolecular complex occurs when the two molecules significantly populate both free and complexed states, and the two states are in rapid exchange. Many protein–ligand interactions fall into this class. Indeed, the structural relationship between ligand and protein

https://doi.org/10.1017/S0033583500003656 Published online by Cambridge University Press

is of primary interest for the field of drug design. Structural characterizations of bound protein–ligand conformations using traditional NMR techniques share many of limitations encountered in the determination of macromolecular complexes; small ligand molecules suffer from lack of protons sufficiently close to the receptor protein to give inter-molecular NOEs. Furthermore, ligand–protein NOEs are often scaled down by exchange between bound and free states.

Several applications have appeared demonstrating the utility of residual dipolar coupling in determining bound-ligand conformations. For example, Fesik and co-workers measured residual dipolar couplings in the tightly bound FKBP/FK506 complex dissolved in colloidal suspension of phage (Olejniczak *et al*. 1999). The residual dipolar coupling strategy that was employed in this case relied on the measurement of natural abundance $^1D_{CH}$ couplings in the ligand molecule, using perdeuterated protein employed to suppress background protein signals. A total of 57 $^1D_{NH}$ dipolar couplings were measured in FKBP, while 23 $^1D_{CH}$ couplings were measured in FK506. These dipolar data were included in a simulated annealing protocol along with previously measured NOE data. The heavy atom rmsd for the ligand molecule (FK506) was reduced from 0·67 Å to 0·29 Å as result of the addition of residual dipolar coupling constraints. Moreover, the accuracy of the NMR structure improved (as judged by the reduction in rmsd when compared to X-ray crystal structure) from 1.12 Å to 0·74 Å.

In another study, Homans and co-workers demonstrated the utility of residual dipolar couplings in determining the conformation of a ^{13}C enriched-trisaccharide ligand Galα1–4Galβ1–4Glc in fast exchange with the B-subunit homopentamer of the toxin derived from *E. coli* 0157 (Shimizu *et al*. 1999). A mixture of the complex (1:5 protein:ligand molar ratios) was partially aligned in a bicelle solution, and $^1D_{CH}$ couplings were measured in the ligand molecule. Small residual dipolar couplings were also observed in the ligand molecule, when using a separate sample that contained bicelle but no protein, indicating that the free ligand itself is also partially aligned. Using dipolar couplings measured in the ligand-only sample as well as the ligand/protein sample, and accounting for the known dissociation constant of the interaction, they were able to extract residual dipolar couplings emanating from the bound state. Using a total of 11 computed bound state dipolar couplings; the authors refined the structure of the trisaccharide using a simulated annealing protocol. The resulting family of structures had an rmsd of less than 0·5 Å for the Galα and Galβ groups, for which five and four residual dipolar couplings were measured respectively, while the Glc group was very disordered due to a lack of orientational data (only two couplings). The determined Galα and Galβ conformation was similar to that observed both in the crystal structure and in a structure determined from a full-relaxation matrix transfer NOE calculation. One noted advantage for the residual dipolar coupling approach was that less material was required than in the previous transfer NOE studies.

Another case involves establishing, not just ligand conformation, but the geometrical relationship of ligand bound to protein using residual dipolar couplings (Bolon *et al*. 1999). The study involved the interaction of Mannose Binding Protein (MBP), a 54 kDa homotrimer composed of three symmetry related carbohydrate recognition domains (CRDs) with the simple sugar α-methyl-mannose (AMM). The binding of AMM to MBP is in fast exchange, and is primarily mediated through the interaction of the 3′ and 4′ hydroxyl groups in the mannose moiety with a calcium atom in the carbohydrate recognition domain.

Using ^{13}C-istopically enriched AMM, five sugar ring $^1D_{CH}$ couplings were measured in

https://doi.org/10.1017/S0033583500003656 Published online by Cambridge University Press

the ligand molecule dissolved in a bicelle solution, both in the presence and absence of MBP. These measurements, along with the knowledge of the binding constant were used to determine dipolar couplings emanating from AMM in the bound state. Using these couplings and knowledge of the pyranose ring sugar conformation, an order matrix apporach was used to determine alignment for AMM in the bound state. In order to determine the geometric relationship of the ligand to the protein, the order tensor orientation from the point of view of MBP also had to be determined. In this case, experimental determination was unnecessary because MBP is a homomultimer with $n = 3$ point group symmetry. This meant that the order tensor would have axial symmetry with the principal direction pointing along the axis of protein symmetry (Al-Hashimi *et al*., 2000*a*). By aligning the experimentally determined principal frame direction for AMM with the C3 symmetry axis of MBP, a structure for AMM bound to MBP was proposed. Interestingly, the determined ligand-bound geometry differed from a geometry determined using modeling studies of an MBP dimer with AMM by as much as 40°. The authors suggested several reasons that may account for this difference, including the presence of an alternate binding site or actual differences in the conformation of MBP between the solution and solid state.

Other interesting applications to ligand exchange include a study by Bax and co-workers on the light activated interaction of an 11-residue synthetic tranducin peptide fragment with the 40 kDa integral membrane protein, rhodopsin (Koenig *et al*. 2000). The peptide itself was modified slightly in this case to push the system more into the fast exchange regime. The interaction between peptide and rhodopsin had been previously studied using solution state transfer NOE studies, however the considerable effects of spin diffusion made it difficult to accurately quantitate data. In the dipolar coupling studies, the protein was strongly oriented because it is organized as part of a field orientable membrane fragment. For the 11-residue synthetic tranducin peptide fragment (S2), ^{15}N-labelled at two positions (Leu 5 and Gly), $^{1}D_{NH}$ couplings were measured in both the free and bound states. These could also be measured in the presence of dark and light adapted states for the protein. Considerable $^{1}H_{N}$ line broadening and a concomitant increase in dipolar contributions to the two observed $^{1}J_{NH}$ couplings were observed under light conditions. A series of 10×9 minute F1-coupled ^{1}H–^{15}N HSQC spectra were recorded showing an exponential decrease in dipolar contributions with time, which parallels the irreversible decay of the peptide-binding meta II state to the peptide non-binding meta III state and finally opsin.

The above are only a sampling of the applications where the measurement of residual dipolar couplings can be of value. They range from complete structure determination in the near absence of other data (Delaglio *et al*. 2000), to the refinement in the presence of other NMR constraints, to determining complexes of both macromolecules and small ligands. For the future, these applications will expand. Hopefully, both the advantages and pitfalls of using dipolar couplings have been illustrated in a way that can guide these future applications.

7. Acknowledgements

The authors would like to thank Dr Homayoun Valafar for preparing Fig. 12, Mark Fischer for preparing Figs. 14–16, Andrew Fowler and Dr Fang Tian for revising the manuscript, Ronald Seidel III for help with references, and all current and former students

of Dr Prestegard's lab. Funding from the NIH, grants GM33225 and RR05351 and NSF grant MCB-97263411 are also acknowledged.

8. References

Al-Hashimi, H. M., Bolon, P. J. & Prestegard, J. H. (2000a). Molecular symmetry as an aid to geometry determination in ligand protein complexes. *J. magn. Reson.* **142**, 153–158.

Al-Hashimi, H. M., Valafar, H., Terrell, M., Zartler, E. R., Eidsness, M. K. & Prestegard, J. H. (2000b). Variation of molecular alignment as a means of resolving orientational ambiguities in protein structures from dipolar couplings. *J. magn. Reson.* **143**, 402–406.

Andrec, M. & Prestegard, J. H. (1998). Metropolis Monte Carlo implementation of Bayesian time-domain parameter estimation: Application to coupling constant estimation from antiphase multiplets. *J. magn. Reson.* **130**, 217–232.

Annila, A., Aitio, H., Thulin, E. & Drakenberg, T. (1999). Recognition of protein folds via dipolar couplings. *J. Biomol. NMR* **14**, 223–230.

Baber, J. L., Libutti, D., Levens, D. & Tjandra, N. (1999). High precision solution structure of the C-terminal KH domain of heterogeneous nuclear ribonucleoprotein K, a c-myc transcription factor. *J. molec. Biol.* **289**, 949–96

Banci, L., Bertini, I., Huber, J. G., Luchinat, C. & Rosato, A. (1998). Partial orientation of oxidized and reduced cytochrome b(5) at high magnetic fields: Magnetic susceptibility anisotropy contributions and consequences for protein solution structure determination. *J. Am. chem. Soc.* **120**, 12903–12909.

Banci, L., Bertini, I., Savellini, G. G., Romagnoli, A., Turano, P., Cremonini, M. A., Luchinat, C. & Gray, H. B. (1997). Pseudocontact shifts as constraints for energy minimization and molecular dynamics calculations on solution structures of paramagnetic metalloproteins. *Proteins Struct. Funct. Genet.* **29**, 68–76.

Barrientos, L. G., Dolan, C. & Gronenborn, A. M. (2000). Characterization of surfactant liquid crystal phases suitable for molecular alignment and measurement of dipolar couplings. *J. biomol. NMR* **16**, 329–337.

Bastiaan, E. W. & MacLean, C. (1990). Molecular orientation in high-field high-resolution NMR. *NMR-Basic Princ. Prog.* **25**, 17–43.

Bastiaan, E. W., Maclean, C., Van Zilj, P. C. M. & Bothner-By, A. A. (1987). High-resolution NMR of liquids and gases: Effects of magnetic-field-induced molecular alignment. *A. Rep. NMR Spec.* **19**, 35–77.

Bax, A. & Tjandra, N. (1997). High-resolution heteronuclear NMR of human ubiquitin in an aqueous liquid crystalline medium. *J. biomol. NMR* **10**, 289–292.

Bax, A., Vuister, G. W., Grzesiek, S., Delaglio, F., Wang, A. C., Tschudin, R. & Zhu, G. (1994). Measurement of homonuclear and heteronuclear J-couplings from quantitative J-correlation. *Meth. Enzymol.* **239**, 79–105.

Bayer, P., Varani, L. & Varani, G. (1999). Refinement of the structure of protein-RNA complexes by residual dipolar coupling analysis. *J. biomol. NMR* **14**, 149–155.

Beger, R. D., Marathias, V. M., Volkman, B. F. & Bolton, P. H. (1998). Determination of internuclear angles of DNA using paramagnetic-assisted magnetic alignment. *J. magn. Reson.* **135**, 256–259.

Bentrop, D., Bertini, I., Cremonini, M. A., Forsen, S., Luchinat, C. & Malmendal, A. (1997). Solution structure of the paramagnetic complex of the N-terminal domain of calmodulin with two Ce^{3+} ions by H-1 NMR. *Biochemistry* **36**, 11605–11618.

Bewley, C. A., Gustafson, K. R., Boyd, M. R., Covell, D. G., Bax, A., Clore, G. M. & Gronenborn, A. M. (1998). Solution structure of cyanovirin-N, a potent HIV-inactivating protein. *Nat. struct. Biol.* **5**, 571–578.

Biekofsky, R. R., Muskett, F. W., Schmidt, J. M., Martin, S. R., Browne, J. P., Bayley, P. M. & Feeney, J. (1999). NMR approaches for monitoring domain orientations in calcium-binding proteins in solution using partial replacement of Ca^{2+} by Tb^{3+}. *FEBS Lett.* **460**, 519–526.

Billeter, M., Neri, D., Otting, G., Qian, Y. Q. & Wüthrich, K. (1993). Precise vicinal coupling constants 3JHNα in proteins from nonlinear fits of J-modulated [15N,1H]-COSY experiments. *J. biomol. NMR* **2**, 257–274.

Bodenhausen, G. & Ernst, R. R. (1981). The accordion experiment, a simple approach to 3-dimensional NMR-spectroscopy. *J. magn. Reson.* **45**, 367–373.

Bolon, P. J., Al-Hashimi, H. M. & Prestegard, J. H. (1999). Residual dipolar coupling derived orientational constraints on ligand geometry in a 53 kDa protein-ligand complex *J. molec. Biol.* **293**, 107–115.

Bothner-By, A. A. (1995). Magnetic field induced alignment of molecules. In *Encyclopedia of Nuclear Magnetic Resonance* (eds. D. M. Grant and R. K. Harris), pp. 2932–2938. Wiley: Chichester.

Bothner-By, A. A., Domaille, P. J. & Gayathri, C. (1981). Ultra-high-field NMR-spectroscopy – observation of proton–proton dipolar coupling in paramagnetic bis[tolyltris(pyrazolyl)borato]cobalt(II). *J. Am. chem. Soc.* **103**, 5602–5603.

Bretthorst, G. L. (1990a). Bayesian-analysis. 1. Parameter-estimation using quadrature NMR models. *J. magn. Reson.* **88**, 533–551.

Bretthorst, G. L. (1990b). Bayesian-analysis. 3. Applications to NMR signal-detection, model selection, and parameter-estimation. *J. magn. Reson.* **88**, 571–595.

Buckingham, A. D. & Pople, J. A. (1963). *Trans. Faraday Soc.* **41**, 2421.

Cai, M., Huang, Y., Zheng, R., Wei, S. Q., Ghirlando, R., Lee, M. S., Craigie, R., Gronenborn, A. M. & Clore, G. M. (1998). Solution structure of the cellular factor BAF responsible for protecting retroviral DNA from autointegration. *Nat. Struct. Biol.* **5**, 903–909.

Cai, M. L., Wang, H., Olejniczak, E. T., Meadows, R. P., Gunasekera, A. H., Xu, N. & Fesik, S. W. (1999). Accurate measurement of H-N-H-alpha residual dipolar couplings in proteins. *J. magn. Reson.* **139**, 451–453.

Carlomagno T, S. H., Rexroth, A., Sorensen, O. W., & Griesinger C. (1998). New methylene specific experiments for the measurement of scalar spin–spin coupling constants between protons attached to C-13. *J. magn. Reson.* **135**, 216–226.

Case, D. A. (1999). Calculations of NMR dipolar coupling strengths in model peptides. *J. biomol. NMR* **15**, 95–102.

Cavagnero, S., Dyson, H. J. & Wright, P. E. (1999). Improved low pH bicelle system for orienting macromolecules over a wide temperature range. *J. biomol. NMR* **13**, 387–391.

Chung, J. & Prestegard, J. H. (1993). Characterization of field-ordered aqueous liquid-crystals by NMR diffusion measurements. *J. phys. Chem.* **97**, 9837–9843.

Chylla, R. A. & Markley, J. L. (1995). Theory and application of the maximum-likelihood principle to NMR parameter-estimation of multidimensional NMR data. *J. biomol. NMR* **5**, 245–258.

Clore, G. M. & Garrett, D. S. (1999). R-factor, free R, and complete cross-validation for dipolar coupling refinement of NMR structures. *J. Am. chem. Soc.* **121**, 9008–9012.

Clore, G. M. & Gronenborn, A. M. (1998). New methods of structure refinement for macromolecular structure determination by NMR. *Proc. natn. Acad. Sci. USA* **95**, 5891–5898.

Clore, G. M., Gronenborn, A. M. & Bar, A. (1998a). A robust method for determining the magnitude of the fully asymmetric alignment tensor of oriented macromolecules in the absence of structural information. *J. magn. Reson.* **133**, 216–221.

Clore, G. M., Gronenborn, A. M. & Tjandra, N. (1998b). Direct structure refinement against residual dipolar couplings in the presence of rhombicity of unknown magnitude. *J. magn. Reson.* **131**, 159–162.

Clore, G. M., Murphy, E. C., Gronenborn, A. M. & Bax, A. (1998c). Determination of three-bond (1)H3′-P-31 couplings in nucleic acids and protein nucleic acid complexes by quantitative J correlation spectroscopy. *J. magn. Reson.* **134**, 164–167.

Clore, G. M., Starich, M. R., Bewley, C. A., Cai, M. L. & Kuszewski, J. (1999). Impact of residual dipolar couplings on the accuracy of NMR structures determined from a minimal number of NOE restraints. *J. Am. chem. Soc.* **121**, 6513–6514.

Clore, G. M., Starich, M. R. & Gronenborn, A. M. (1998d). Measurement of residual dipolar couplings of macromolecules aligned in the nematic phase of a colloidal suspension of rod- shaped viruses. *J. Am. chem. Soc.* **120**, 10571–10572.

Contreras, M. A., Ubach, J., Millet, O., Rizo, J. & Pons, M. (1999). Measurement of one bond dipolar couplings through lanthanide- induced orientation of a calcium-binding protein. *J. Am. chem. Soc.* **121**, 8947–8948.

de Alba, E., Baber, J. L. & Tjandra, N. (1999). The use of residual dipolar coupling in concert with backbone relaxation rates to identify conformational exchange by NMR. *J. Am. chem. Soc.* **121**, 4282–4283.

Delaglio, F., Kontaxis, G. & Bax, A. (2000). Protein structure determination using molecular fragment replacement and NMR dipolar couplings. *J. Am. chem. Soc.* **122**, 2142–2143.

Demene, H., Tsan, P., Gans, P. & Marion, D. (2000). NMR determination of the magnetic susceptibility anisotropy of cytochrome c′ of Rhodobacter capsulatus by (1)J(HN) dipolar coupling constants measurement: Characterization of its monomeric state in solution. *J. phys. Chem. B* **104**, 2559–2569.

Emsley, I. W. & Lindon, J. C. (1975). *NMR Spectroscopy Using Liquid Crystal Solvents*. Pergamon Press: Oxford.

Emsley, L. & Bodenhausen, G. (1990). Gaussian pulse cascades – new analytical functions for rectangular selective inversion and in-phase excitation in NMR. *Chem. Phys. Lett.* **165**, 469–476.

Ernst, R. R., Bodenhausen, G. & Wokaun, A. (1987). *Principles of Nuclear Magnetic Resonance in One and Two Dimensions*. Clarendon Press, Oxford.

Facke, T. & Berger, S. (1996). Alpha/beta-ge-SELINCOR-TOCSY, a new method for the determination of H,C coupling constants. *J. magn. Reson. Ser. A* **119**, 260–263.

Fischer, M. W. F., Losonczi, J. A., Weaver, J. L. & Prestegard, J. H. (1999). Domain orientation and dynamics in multidomain proteins from residual dipolar couplings. *Biochemistry* **38**, 9013–9022.

Fushman, D., Xu, R. & Cowburn, D. (1999). Direct determination of changes of interdomain orientation on ligation: Use of the orientational dependence of N-15 NMR relaxation in Abl SH(32). *Biochemistry* **38**, 10225–10230.

Garrett, D. S., Powers, R., Gronenborn, A. M. & Clore, G. M. (1991). A common sense approach to peak picking in two-, three-, and four-dimensional spectra using automatic computer analysis of contour diagrams. *J. magn. Reson.* **95**, 214–220.

Garrett, D. S., Seok, Y. J., Peterkofsky, A., Gronenborn, A. M. & Clore, G. M. (1999). Solution structure of the 40,000 M-r phosphoryl transfer complex between the N-terminal domain of enzyme I and HPr. *Nat. struct. Biol.* **6**, 166–173.

Ghose, R. & Prestegard, J. H. (1997). Electron spin-nuclear spin cross-correlation effects on multiplet splittings in paramagnetic proteins. *J. magn. Reson.* **128**, 138–143.

Girvin, M. E. (1994). Increased sensitivity of COSY spectra by use of constant-time T(1) periods (CT COSY). *J. magn. Reson. Ser. A* **108**, 99–102.

Griesinger, C. & Ernst, R. R. (1987). Frequency offset effects and their elimination in NMR rotating-frame cross-relaxation spectroscopy. *J. magn. Reson.* **75**, 261–271.

Griesinger, C., Sorensen, O. W. & Ernst, R. R. (1985). Two-dimensional correlation of connected NMR transitions. *J. Am. chem. Soc.* **107**, 6394–6396.

Griesinger, C., Sorensen, O. W. & Ernst, R. R. (1986). Correlation of connected transitions by two-dimensional NMR-spectroscopy. *J. chem. Phys.* **85**, 6837–6852.

Hansen, M. R., Hanson, P. & Pardi, A. (2000). Filamentous bacteriophage for aligning RNA, DNA, and proteins for measurement of nuclear magnetic resonance dipolar coupling interactions. *Method Enzy-mol.* **317**, 220–240.

Hansen, M. R., Mueller, L. & Pardi, A. (1998). Tunable alignment of macromolecules by filamentous phage yields dipolar coupling interactions. *Nat. struct. Biol.* **5**, 1065–1074.

Hare, B. J., Prestegard, J. H. & Engelman, D. M. (1995). Small angle X-ray scattering studies of magnetically oriented lipid bilayers. *Biophys. J.* **69**, 1891–1896.

Heikkinen, S. A. H., Permi, P., Folmer, R., Lappalainen, K. & Kilpelainen, I. (1999). J-multiplied HSQC (MJ-HSQC): A new method for measuring (3)J(HNH alpha) couplings in N-15-labeled proteins. *J. magn. Reson.* **137**, 243–246.

Hitchens, T. K., McCallum, S. A. & Rule, G. S. (1999). A J(CH)-modulated 2D (HACACO)NH pulse scheme for quantitative measurement of C-13(alpha)–H-1(alpha) couplings in N-15, C-13-labeled proteins. *J. magn. Reson.* **140**, 281–284.

Hoogstraten, C. G. & Pardi, A. (1998). Measurement of carbon-phosphorus J coupling constants in RNA using spin-echo difference constant-time HCCH-COSY. *J. magn. Reson.* **133**, 236–240.

Horrocks, W. D. & Sipe, J. P. (1972). Lanthanide complexes as nuclear magnetic resonance structural probes – paramagnetic anisotropy of shift reagent adducts. *Science* **177**, 994–996.

Kiddle, G. R. & Homans, S. W. (1998). Residual dipolar couplings as new conformational restraints in isotopically C-13-enriched oligosaccharides. *FEBS Lett.* **436**, 128–130.

Kleywegt, G. J., Vuister, G. W., Padilla, A., Kneg-tel, R. M. A., Boelens, R. & Kaptein, R. (1993). Computer-assisted assignment of homonuclear-3d NMR-spectra of proteins – application to pike parv-albumin-Iii. *J. magn. Reson. Ser. B* **102**, 166–176.

Koenig, B. W., Hu, J. S., Ottiger, M., Bose, S., Hendler, R. W. & Bax, A. (1999). NMR measurement of dipolar couplings in proteins aligned by transient binding to purple membrane fragments. *J. Am. chem. Soc.* **121**, 1385–1386.

Koenig, B. W., Mitchell, D. C., Konig, S., Grzesiek, S., Litman, B. J. & Bax, A. (2000). Measurement of dipolar couplings in a transducin peptide fragment weakly bound to oriented photo-activated rhodopsin. *J. biomol. NMR* **16**, 121–125.

Lisicki, M. A., Mishra, P. K., Bothnerby, A. A. & Lindsey, J. S. (1988). Solution conformation of a porphyrin quinone cage molecule determined by dipolar magnetic-field effects in ultra-high-field NMR. *J. phys. Chem.* **92**, 3400–3403.

Lohman, J. A. B. & MacLean, C. (1978). Alignment effects on high resolution NMR spectra, induced by the magnetic field. *Chem. Phys.* **35**, 269–274.

Losonczi, J. A., Andrec, M., Fischer, M. W. F. & Prestegard, J. H. (1999). Order matrix analysis of residual dipolar couplings using singular value decomposition. *J. magn. Reson.* **138**, 334-342.

Losonczi, J. A. & Prestegard, J. H. (1998a). Improved dilute bicelle solutions for high-resolution NMR of biological macromolecules. *J. biomol. NMR* **12**, 447–451.

Losonczi, J. A. & Prestegard, J. H. (1998b). Nuclear magnetic resonance characterization of the myristoylated, N-terminal fragment of ADP-ribosylation factor 1 in a magnetically oriented membrane array. *Biochemistry* **37**, 706–716.

Markus, M. A., Gerstner, R. B., Draper, D. E. & Torchia, D. A. (1999). Refining the overall structure and subdomain orientation of ribosomal protein S4 Delta 41 with dipolar couplings measured by NMR in uniaxial liquid crystalline phases. *J. molec. Biol.* **292**, 375–387.

Martin, Y. L. (1994). A global approach to accurate and automatic quantitative-analysis of NMR-spectra

by complex least-squares curve-fitting. *J. magn. Reson. Ser. A* **111**, 1–10.

Martin-Pastor, M. & Bush, C. A. (2000). Conformational studies of human milk oligosaccharides using H-1-C-13 one-bond NMR residual dipolar couplings. *Biochemistry* **39**, 4674–4683.

Meiler, J., Blomberg, N., Nilges, M. & Griesinger, C. (2000). A new approach for applying residual dipolar couplings as restraints in structure elucidation. *J. biomol. NMR* **16**, 245–252.

Meissner, A., Duus, J. O. & Sorensen, O. W. (1997a). Integration of spin-state-selective excitation into 2D NMR correlation experiments with heteronuclear ZQ/2Q pi rotations for (1)J(XH)-resolved E.COSY-type measurement of heteronuclear coupling constants in proteins. *J. biomol. NMR* **10**, 89–94.

Meissner, A., Duus, J. O. & Sorensen, O. W. (1997b). Spin-state-selective excitation. Application for E.COSY-type measurement of J(HH) coupling constants. *J. magn. Reson.* **128**, 92–97.

Miller, M. I., Chen, S. C., Kuefler, D. A. & Davignon, D. A. (1993). Maximum-likelihood and the em algorithm for 2d NMR-spectroscopy. *J. magn. Reson. Ser. A* **104**, 247–257.

Moltke, S. & Grzesiek, S. (1999). Structural constraints from residual tensorial couplings in high resolution NMR without an explicit term for the alignment tensor. *J. biomol. NMR* **15**, 77–82.

Montelione, G. T. & Wagner, G. (1989). Accurate measurements of homonuclear HN-Hα coupling constants in polypeptides using heteronuclear 2D NMR experiments. *J. Am. chem. Soc.* **111**, 5474–5475.

Nilges, M., Gronenborn, A. M., Brunger, A. T. & Clore, G. M. (1988). Determination of 3-dimensional structures of proteins by simulated annealing with interproton distance restraints – application to crambin, potato carboxypeptidase inhibitor and barley serine proteinase inhibitor-2. *Protein Eng.* **2**, 27–38.

O'Donoghue, S. & Nilges, M. (1999). *Calculation of Symmetric Oligomer Structures from NMR Data*. Plenum: New York.

Ojennus, D. D., Mitton-Fry, R. M. & Wuttke, D. S. (1999). Induced alignment and measurement of dipolar couplings of an SH2 domain through direct binding with filamentous phage. *J. Biomol. NMR* **14**, 175–179.

Olejniczak, E. T., Meadows, R. P., Wang, H., Cai, M. L., Nettesheim, D. G. & Fesik, S. W. (1999). Improved NMR structures of protein/ligand complexes using residual dipolar couplings. *J. Am. chem. Soc.* **121**, 9249–9250.

Ottiger, M. & Bax, A. (1998). Characterization of magnetically oriented phospholipid micelles for measurement of dipolar couplings in macromolecules. *J. biomol. NMR* **12**, 361–372.

Ottiger, M. & Bax, A. (1999). Bicelle-based liquid crystals for NMR-measurement of dipolar couplings at acidic and basic pH values. *J. biomol. NMR* **13**, 187–191.

Ottiger, M., Delaglio, F. & Bax, A. (1998a). Measurement of J and dipolar couplings from simplified two-dimensional NMR spectra. *J. magn. Reson.* **131**, 373–378.

Ottiger, M., Delaglio, F., Marquardt, J. L., Tjandra, N. & Bax, A. (1998b). Measurement of dipolar couplings for methylene and methyl sites in weakly oriented macromolecules and their use in structure determination. *J. magn. Reson.* **134**, 365–369.

Pellecchia, M., Vander Kooi, C. W., Keliikuli, K. & Zuiderweg, E. R. P. (2000). Magnetization transfer via residual dipolar couplings: Application to proton–proton correlations in partially aligned proteins. *J. magn. Reson.* **143**, 435–439.

Permi, P. & Annila, A. (2000). Transverse relaxation optimised spin-state selective NMR experiments for measurement of residual dipolar couplings. *J. biomol. NMR* **16**, 221–227.

Pervushin, K., Riek, R., Wider, G. & Wüthrich, K. (1997). Attenuated T-2 relaxation by mutual cancellation of dipole- dipole coupling and chemical shift anisotropy indicates an avenue to NMR structures of very large biological macromolecules in solution. *Proc. natn. Acad. Sci. USA* **94**, 12366–12371.

Peti, W. & Griesinger, C. (2000). Measurement of magnitude and sign of H,H-dipolar couplings in proteins. *J. Am. chem. Soc.* **122**, 3975–3976.

Ponstingl H. O. G. (1998). Rapid measurement of scalar three-bond H-1(N)-H-1(alpha) spin coupling constants in N-15-labelled proteins. *J. biomol. NMR* **12**, 319–324.

Prestegard, J. H. (1998). New techniques in structural NMR – anisotropic interactions. *Nat. struct. Biol.* **5**, 517–522.

Prestegard, J. H., Tolman, J. R., Al-Hashimi, H. M. & Andrec, M. (1999). Protein structure and dynamics from field induced residual dipolar couplings. In *Biological Magnetic Resonance*, *vol. 17. Structure Computation and Dynamics in Protein NMR* (eds. N. R. Krishna and L. J. Berliner), pp. 311–355. Plenum: New York.

Prosser, R. S., Hunt, S. A., DiNatale, J. A. & Vold, R. R. (1996). Magnetically aligned membrane model sysytems with positive order parameter: switching the sign of Szz with paramagnetic ions. *J. Am. chem. Soc.* **118**, 269–270.

Prosser, R. S., Losonczi, J. A. & Shiyanovskaya, I. V. (1998a). Use of a novel aqueous liquid crystalline medium for high-resolution NMR of macromolecules in solution. *J. Am. chem. Soc.* **120**, 11010–11011.

Prosser, R. S., Volkov, V. B. & Shiyanovskaya, I. V. (1998b). Novel chelate-induced magnetic alignment of biological membranes. *Biophys. J.* **75**, 2163–2169.

Ram, P., Mazzola, L. & Prestegard, J. H. (1989). Orientational analysis of micelle-associated trehalose using an NMR-pseudoenergy approach. *J. Am. chem. Soc.* **111**, 3176–3182.

Ram, P. & Prestegard, J. H. (1988). Magnetic-field induced ordering of bile-salt phospholipid micelles – new media for NMR structural investigations. *Biochim. biophys. Acta* **940**, 289–294.

Ramirez, B. E. & Bax, A. (1998). Modulation of the alignment tensor of macromolecules dissolved in a dilute liquid crystalline medium. *J. Am. chem. Soc.* **120**, 9106–9107.

Ross, A., Czisch, M. & Holak, T. A. (1996). Selection of simultaneous coherence pathways with gradient pulses. *J. magn. Reson. Ser. A* **118**, 221–226.

Rundlof, T., Landersjo, C., Lycknert, K., Maliniak, A. & Widmalm, G. (1998). NMR investigation of oligosaccharide conformation using dipolar couplings in an aqueous dilute liquid crystalline medium. *Magn. Reson. Chem.* **36**, 773–776.

Sanders, C. R., Hare, B. J., Howard, K. P. & Prestegard, J. H. (1994). Magnetically-oriented phospholipid micelles as a tool for the study of membrane-associated molecules. *Prog. nucl. magn. Reson. Spectrosc.* **26**, 421–444.

Sanders, C. R. & Prestegard, J. H. (1990). Magnetically orientable phospholipid-bilayers containing small amounts of a bile-salt analog, Chapso. *Biophys. J.* **58**, 447–460.

Sanders, C. R. & Prosser, R. S. (1998). Bicelles: a model membrane system for all seasons? *Struct. Fold. Des.* **6**, 1227–1234.

Sanders, C. R. & Schwonek, J. P. (1992). Characterization of magnetically orientable bilayers in mixtures of dihexanoylphosphatidylcholine and dimyristoylphosphatidylcholine by solid-state NMR. *Biochemistry* **31**, 8898–8905.

Sass, J., Cordier, F., Hoffmann, A., Cousin, A., Omichinski, J. G., Lowen, H. & Grzesiek, S. (1999). Purple membrane induced alignment of biological macromolecules in the magnetic field. *J. Am. chem. Soc.* **121**, 2047–2055.

Saupe, A. (1964). *Z. Naturfors.* **19a**, 161.

Saupe, A. (1968). Recent results in the field of liquid crystals. *Angew. Chem. Int. Ed. Engl.* **7**, 97–112.

Saupe, A. & Englert, G. (1963). High-resolution nuclear magnetic resonance spectra of oriented molecules. *Phys. Rev. Lett.* **11**, 462–464.

Shimizu, H., Donohue-Rolfe, A. & Homans, S. W. (1999). Derivation of the bound-state conformation of a ligand in a weakly aligned ligand–protein complex. *J. Am. chem. Soc.* **121**, 5815–5816.

Skalicky, J. J., Gibney, B. R., Rabanal, F., Urbauer, R. J. B., Dutton, P. L. & Wand, A. J. (1999). Solution structure of a designed four-alpha-helix bundle maquette scaffold. *J. Am. chem. Soc.* **121**, 4941–4951.

Skrynnikov, N. R., Goto, N. K., Yang, D. W., Choy, W. Y., Tolman, J. R., Mueller, G. A. & Kay, L. E. (2000). Orienting domains in proteins using dipolar couplings measured by liquid-state NMR: Differences in solution and crystal forms of maltodextrin binding protein loaded with beta-cyclodextrin. *J. molec. Biol.* **295**, 1265–1273.

Snyder, L. C. (1965). Analysis of nuclear magnetic resonance spectra of molecules in liquid-crystal solvents. *J. chem. Phys.* **43**, 4041–4050.

Tian, F., Bolon, P. J. & Prestegard, J. H. (1999). Intensity-based measurement of homonuclear residual dipolar couplings from CT-COSY. *J. Am. chem. Soc.* **121**, 7712–7713.

Tjandra, N. (1999). Establishing a degree of order: obtaining high-resolution NMR structures from molecular alignment. *Struct. Fold. Des.* **7**, R205–R211.

Tjandra, N. & Bax, A. (1997a). Direct measurement of distances and angles in biomolecules by NMR in a dilute liquid crystalline medium. *Science* **278**, 1111–1114.

Tjandra, N. & Bax, A. (1997b). Direct measurement of distances and angles in biomolecules by NMR in a dilute liquid crystalline medium (vol 278, pg 1111, 1997). *Science* **278**, 1697–1697.

Tjandra, N. & Bax, A. (1997c). Measurement of dipolar contributions to (1)J(CH) splittings from magnetic-field dependence of J modulation in two-dimensional NMR spectra. *J. magn. Reson.* **124**, 512–515.

Tjandra, N., Grzesiek, S., Pastor, R. W. & Bax, A. (1996). Anisotropic diffusion and orientation of proteins in solution studied by heteronuclear NMR. *Prog. Biophys. molec. Biol.* **65**, SH402.

Tjandra, N., Omichinski, J. G., Gronenborn, A. M., Clore, G. M. & Bax, A. (1997). Use of dipolar H-1-N-15 and H-1-C-13 couplings in the structure determination of magnetically oriented macromolecules in solution. *Nat. struct. Biol.* **4**, 732–738.

Tolman, J. R., Flanagan, J. M., Kennedy, M. A. & Prestegard, J. H. (1995). Nuclear magnetic dipole interactions in field-oriented proteins – information for structure determination in solution. *Proc. natn. Acad. Sci. USA* **92**, 9279–9283.

Tolman, J. R., Flanagan, J. M., Kennedy, M. A. & Prestegard, J. H. (1997). NMR evidence for slow collective motions in cyanometmyoglobin. *Nat. struct. Biol.* **4**, 292–297.

Tolman, J. R. & Prestegard, J. H. (1996a). Measurement of amide N-15-H-1 one-bond couplings in proteins using accordion heteronuclear-shift-correlation experiments. *J. magn. Reson. Ser. B* **112**, 269–274.

Tolman, J. R. & Prestegard, J. H. (1996b). A quantitative J-correlation experiment for the accurate measurement of one-bond amide N-15–H-1 couplings in proteins. *J. magn. Reson. Ser. B* **112**, 245–252.

Tsui, V., Zhu, L. M., Huang, T. H., Wright, P. E. & Case, D. A. (2000). Assessment of zinc finger orientations by residual dipolar coupling constants. *J. biomol. NMR* **16**, 9–21.

Van Vleck, J. H. (1932). *The Theory of Electric and Magnetic Susceptibilities*. Oxford University Press: Oxford.

Vold, R. R. & Prosser, R. S. (1996). Magnetically oriented phospholipid bilayered micelles for structural studies of polypeptides. Does the ideal bicelle exist? *J. magn. Reson. Ser. B* **113**, 267–271.

Volkman, B. F., Wilkens, S. J., Lee, A. L., Xia, B., Westler, W. M., Beger, R. & Markley, J. L. (1999). Redox-dependent magnetic alignment of Clostridium pasteurianum rubredoxin: Measurement of magnetic susceptibility anisotropy and prediction of pseudocontact shift contributions. *J. Am. chem. Soc.* **121**, 4677–4683.

Vuister, G. W. & Bax, A. (1993). Quantitative J correlation: a new approach for measuring homonuclear three-bond J(HNHα) coupling constants in 15N-enriched proteins. *J. Am. chem. Soc.* **115**, 7772–7777.

Wang, H., Eberstadt, M., Olejniczak, E. T., Meadows, R. P. & Fesik, S. W. (1998a). A liquid crystalline medium for measuring residual dipolar couplings over a wide range of temperatures. *J. Biomol. NMR* **12,** 443–446.

Wang, Y., Marquardt, J. L., Winglfield, P., Stahl, S. J., Lee-Huang, S., Torchia, D. & Bax, A. (1998b). Simultaneous measurement of 1H–15N, 1H–13C′, and 15N–13C′ dipolar couplings in a perdeuterated 30 kDa protein dissolved in a dilute liquid crystalline phase. *J. Am. chem. Soc.* **120**, 7385–7386.

Wang, Y. X., Neamati, N., Jacob, J., Palmer, I., Stahl, S. J., Kaufman, J. D., Huang, P. L., Winslow, H. E., Pommier, Y., Wingfield, P. T., Lee-Huang, S., Bax, A. & Torchia, D. A. (1999). Solution structure of anti-HIV-1 and anti-tumor protein MAP30: Structural insights into its multiple functions. *Cell* **99**, 433–442.

Weaver, J. L. & Prestegard, J. H. (1998). Nuclear magnetic resonance structural and ligand binding studies of BLBC, a two-domain fragment of barley lectin. *Biochemistry* **37**, 116–128.

Weyl, H. (1952). Symmetry. Princeton University Press: Princeton.

Willker, W. & Leibfritz, D. (1992). Accurate measurement of homonuclear coupling-constants using Jhh-TOCSY. *J. Magn. Reson.* **99**, 421–425.

Wüthrich, K. (1986). *NMR of Proteins and Nucleic Acids*. Wiley: New York.

Yang, D. W., Tolman, J. R., Goto, N. K. & Kay, L. E. (1998). An HNCO-based pulse scheme for the measurement of C-13(alpha)–H-1(alpha) one-bond dipolar couplings in N-15, C-13 labeled proteins. *J. biomol. NMR* **12**, 325–332.

Yang, D. W., Venters, R. A., Mueller, G. A., Choy, W. Y. & Kay, L. E. (1999). TROSY-based HNCO pulse sequences for the measurement of (HN)-H- 1-N-15, N-15-(CO)-C-13, (HN)-H-1-(CO)-C-13, (CO)-C-13-C-13(alpha) and (HN)-H-1-C-13(alpha) dipolar couplings in N-15, C-13, H-2-labeled proteins. *J. biomol. NMR* **14**, 333–343.